Glacitectonism, subglacial and glacilacustrine processes during a Neoproterozoic panglaciation, north-east Svalbard

Fleming, Edward J.; Benn, Douglas I; Stevenson, Carl T. E.; Petronis, Michael S.; Hambrey, Michael; Fairchild, Ian J.

Published in:
Sedimentology

DOI:
10.1111/sed.12251

Publication date:
2016

Citation for published version (APA):
Fleming, E. J., Benn, D. I., Stevenson, C. T. E., Petronis, M. S., Hambrey, M., & Fairchild, I. J. (2016). Glacitectonism, subglacial and glacilacustrine processes during a Neoproterozoic panglaciation, north-east Svalbard. *Sedimentology*, *63*(2), 411-442. https://doi.org/10.1111/sed.12251

Received Date : 19-Dec-2014

Revised Date : 09-Sep-2015

Accepted Date : 02-Nov-2015

Article type : Original Manuscript

Glacitectonism, subglacial and glacilacustrine processes during a Neoproterozoic panglaciation, north-east Svalbard

Edward J. Fleming*[1,2,6]

Douglas I. Benn[2,3]

Carl T.E. Stevenson[1]

Michael S. Petronis[4]

Michael J. Hambrey[5]

Ian J. Fairchild[1]

[1] School of Geography, Earth and Environmental Sciences, University of Birmingham, Birmingham B15 2TT, UK

[2] Department of Geology, the University Centre in Svalbard (UNIS Longyearbyen), Norway

[3] Department of Geography and Sustainable Development, University of St Andrews, UK.

[4] Natural Resource Management, New Mexico Highlands University, Las Vegas, NM, USA

This is an Accepted Article that has been peer-reviewed and approved for publication in the *Sedimentology*, but has yet to undergo copy-editing and proof correction. Please cite this article as an "Accepted Article"; doi: 10.1111/sed.12251

[5] Centre for Glaciology, Department of Geography and Earth Sciences, Aberystwyth University, Aberystwyth, Ceredigion, SY23 3DB, UK

[6] Present address: CASP, University of Cambridge, 181a Huntingdon Road, Cambridge CB3 0DH, England, UK

*Corresponding Author. Tel.: +44 (0)1223 760700 E-mail address: edward.fleming@casp.cam.ac.uk (E.J. Fleming)

Associate Editor – Dan Le Heron

Short Title – Glacitectonism in a Neoproterozoic panglaciation

ABSTRACT

Palaeoenvironmental reconstruction of Neoproterozoic successions has been the subject of long-standing debate, particularly concerning the interpretation of diamictites. The Wilsonbreen Formation of north-east Svalbard is a 130 to 180 m thick diamictite-dominated glacigenic succession deposited during a late Cryogenian (Marinoan) glaciation. Previous research has highlighted a complex sedimentary architecture with evidence of subaqueous, subglacial and non-glacial conditions. This study combines well-established sedimentological techniques with the first sedimentological application of the anisotropy of magnetic susceptibility (AMS) technique in Neoproterozoic glacial sediments, to investigate the origin and palaeoenvironmental significance of glacigenic sediments within the Wilsonbreen Formation. A range of lithofacies occurs within the succession, dominated by massive diamictites, sandstones and conglomerates. Some of these facies display evidence of primary deformation and can be grouped into a Deformed Facies Association; these are interpreted to have been formed through glacitectonic deformation in a subglacial environment. Fabric investigation reveals that this deformation was associated with glacier flow towards the north. In addition, an Undeformed Facies Association records deposition in ice-proximal

and ice-distal subaqueous environments. Taken together with intervening non-glacial facies, the glacigenic sediments record a series of advance–retreat cycles, with ice flow involving sliding and sediment shearing below wet-based ice.

Keywords: Anisotropy of magnetic susceptibility, Cryogenian, glacitectonism, Snowball Earth, subglacial

1. INTRODUCTION

The aim of this paper is to evaluate the evolution of one of the best-preserved Cryogenian glacigenic successions in the Northern Hemisphere, and in particular the newly recognised role played by glacitectonism. This then allows the authors to throw light on inferred 'Snowball Earth' conditions, with which these strata have long been associated. In a companion paper, Fairchild et al. (2015) investigate the carbonates that are intimately associated with these glacigenic deposits. Together, this research provides new insights concerning the role of the Snowball Earth Theory in explaining geological evolution at the end of the Cryogenian Period.

The Wilsonbreen Formation of north-east Svalbard is composed of up to 180 m of exceptionally well-preserved glacigenic sediments, deposited during the second of two Neoproterozoic panglaciations, where ice sheets existed on all continents at all latitudes (Hoffman, 2009). This period of glaciation is now equated with the Marinoan glaciation of South Australia, and the panglaciation of the same name (Halverson et al., 2004). Previous interpretations of these Marinoan deposits have suggested an interplay of glacial processes representing both subaqueous and subglacial environments (Fairchild & Hambrey, 1984, 1995). In the present study, the origin and significance of these deposits is investigated in detail. Processes of sediment transport, deposition and deformation were

determined using a combination of facies analysis, structural geology, clast shape and macrofabric analysis, and the anisotropy of magnetic susceptibility (AMS) technique.

Massive diamictites, such as those that dominate the Wilsonbreen Formation, are inherently difficult to interpret (Eyles & Januszczak, 2004). This is, in part, because similar properties can develop in various depositional environments, including glacial (glacimarine, glacilacustrine, subglacial and proglacial) and non-glacial (Dowdeswell et al., 1985) settings. Research on the Wilsonbreen Formation to date has provided a broad depositional interpretation (e.g. Hambrey et al., 1981; Fairchild & Hambrey, 1984); however, uncertainty exists over the precise glacidepositional regimes that occurred and their association with Neoproterozoic climatic conditions.

Since the previous research on the Wilsonbreen was undertaken, there have been significant advances in the understanding of the processes leading to the deposition of till (Benn & Evans, 2010, and references therein). There is now a greater knowledge of sediment assemblages associated with different depositional environments (e.g. Evans, 2005), which enables reliable palaeoenvironmental interpretations to be made with reference to the modern sedimentary record.

Glacigenic deformation structures (for example, glacitectonites) are now also better understood than in the early 1980s (Benn & Evans, 1996; van der Wateren, 2002; Aber & Ber, 2007). Glacitectonic structures are common in both modern and Quaternary sediments and have also been observed in many pre-Quaternary sediments (e.g. Le Heron et al., 2005; Benn & Prave, 2006; Busfield & Le Heron, 2013). Analysis of these structures can provide important information about genetic environments and deformational histories.

New techniques have also been developed for understanding glacial sediments. Of these, AMS analysis has been applied to tills by several authors (e.g. Fuller, 1962; Stupavsky & Gravenor, 1975; Eyles et al., 1987) and it has been shown that, in conjunction with other petrofabric techniques, AMS can provide invaluable information on the formation and subsequent deformation of glacial

sediments particularly where visible structures are lacking. In recent years, the technique has been applied to a variety of topics in glacial geology, such as in the determination of palaeoflow from subglacial sediments (Shumway & Iverson, 2009; Thomason & Iverson, 2009; Gentoso et al., 2012), investigations of glacitectonism (Fleming et al., 2013b) and deformation within debris-rich basal ice (Fleming et al., 2013a).

Utilising current understanding of depositional environments, combined with the novel application of the AMS technique, it is possible to extract detailed information from the glacial facies of the Wilsonbreen Formation. The objectives of this study are to: (i) describe the glacial lithofacies observed within the succession in terms of their facies associations; (ii) determine the origin of the soft-sediment deformation features (glacitectonic or slumping); and finally (iii) use a combination of clast fabric analysis and the application of AMS to identify strain signatures and preferred orientations within the sediment to determine ice flow and sediment transport directions. The present paper focuses on well-exposed sections at Reinsryggen, Andromedafjellet, Dracoisen and Ditlovtoppen (Fig. 1). An overview of the Wilsonbreen Formation and an assessment of its significance for the Snowball Earth theory are provided by Benn et al. (2015).

2. GEOLOGICAL BACKGROUND

The Polarisbreen Group (Fig. 2) is a Neoproterozoic mixed siliciclastic-carbonate unit and forms part of the Heckla Hoek tectono-sedimentary sequence of north-east Svalbard (Fig. 1), a 7 km thick succession of Neoproterozoic to Ordovician sedimentary strata and metamorphic rocks exposed along a Caledonian fold belt. The Svalbard archipelago (Fig. 1) consists of three tectonic terranes juxtaposed during the Caledonian Orogeny (Harland, 1971; Harland et al., 1992; Lyberis & Manby, 1993). The relatively undeformed Hecla Hoek succession is exposed on the northern part of the Eastern Terrane. The section has been correlated with the southern north-east Greenland Caledonides, suggesting an origin on the Laurentian margin (Fairchild & Hambrey, 1995).

Sedimentation of the Hecla Hoek succession was probably related to the breakup of Rodinia (Halverson et al., 2004). After the initial deposition of the siliciclastic Veteranen Group, a broad carbonate platform developed in a slowly subsiding basin opening towards the south (Halverson et al., 2004). Following this, renewed subsidence has been suggested to have followed, based on basin-deepening in Northeast Greenland and the deposition of the mostly siliciclastic Polarisbreen Group of which the Wilsonbreen Formation forms part.

The Polarisbreen Group (Fig. 2) is divided into three formations (Elbobreen, Wilsonbreen and Dracoisen), conformably overlying the Akademikerbreen Group and underlying the Cambrian Tokammane Formation (Harland et al., 1993). Two major glacigenic units have been described; an older, Petrovbreen Member (E2) of the Elbobreen Formation and the younger Wilsonbreen Formation (Fairchild and Hambrey, 1984). These are closely correlated with diamictite pairs in Northeast Greenland (Kulling, 1934; Knoll et al., 1986; Fairchild & Hambrey, 1995) and are very similar to other diamictite pairs in the North Atlantic region, although geochronological evidence is commonly lacking which precludes accurate correlation (Hambrey, 1983). The Wilsonbreen Formation is the younger and thicker glacial interval within the Polarisbreen Group, consisting of up to 130 to 180 m of a grey to maroon, massive to weakly bedded diamictite-dominated unit overlying the Slangen Member in the south and the Bråvika Member in the north (which thins and becomes absent in the south) and underlying the Dracoisen Formation (Halverson et al., 2004).

The Wilsonbreen Formation was key in the development of the early ideas about widespread glaciation in the Neoproterozoic (Kulling, 1934; Harland, 1964; Harland & Rudwick, 1964; Hambrey, 1992) and throughout the latter part of the 20th Century, the glacigenic rocks of the Polarisbreen Group were subject to various sedimentological studies (e.g. Chumakov, 1968; Hambrey et al., 1981; Hambrey, 1982; Fairchild, 1983; Fairchild & Hambrey, 1984; Fairchild et al., 1989; Harland et al., 1993). After the strong advocation of Snowball Earth theory (Hoffman et al., 1998), geochemical and stratigraphic analyses of Halverson et al. (2004) were used to argue that the glacigenic sediments of

the Polarisbreen Group were deposited within a single global glaciation. However, Halverson et al. (2007) and Hoffman et al. (2012) subsequently revisited the succession and reinterpreted it as representing two Snowball Earth panglaciations.

The Wilsonbreen Formation is subdivided into the Ormen (W1), Middle Carbonate (W2) and Gropbreen (W3) members (Hambrey, 1982). The W1 member consists mostly of poorly stratified diamictite, but also includes lenses and interbeds of sandstone, conglomerate and breccia. The Middle Carbonate Member is marked by the presence of precipitated carbonates, interbedded with clastic fluvial and lacustrine facies and diamictite. The W3 Member is lithologically similar to W1 and consists of massive to weakly stratified diamictite with interbedded sandstones. The overall depositional setting was a large, closed lacustrine basin that underwent repeated cycles of desiccation and flooding (Benn et al., 2015). Detailed descriptions and interpretations of the carbonate and associated facies in the W2 Member (Fig. 1) are provided by Fairchild et al. (this issue).

3. METHODS

Sections through the Wilsonbreen Formation were examined and logged at Dracoisen, Ditlovtoppen, Andromedafjellet and Reinsryggen in north-east Svalbard (Fig. 1 and 2) during the summer 2010 and 2011 field seasons. Sections were analysed following the lithofacies approach, originally developed for fluvial sediments by Miall (1977), adapted for glacial sediments by Eyles et al. (1983) and subsequently modified for the present study where necessary. Diamictites were classified using the scheme developed by Moncrieff (1989) and modified by Hambrey (1994), based on the relative proportions of gravel, sand and mud (silt and clay). In this scheme, diamictites are defined as rocks that contain 1 to 50% gravel with a matrix comprising greater than 10% of sand, mud or both sand and mud.

In many places, diamictites of the Wilsonbreen Formation are friable, allowing included clasts to be removed intact from the surrounding matrix. This permitted measurements of both clast morphology and orientation, using methods developed for unlithified sediments. Clast morphology (shape, roundness and surface texture) was measured for samples of 50 clasts taken from diamictites of the W1, W2 and W3 members, and compared with control samples of known origin to determine transport pathways (Benn & Ballantyne, 1994; Lukas et al., 2013). Clast shape was determined by measuring the long (a), intermediate (b) and short (c) axes of individual clasts. These data are displayed on triangular diagrams following the methods of Sneed & Folk (1958) and Benn & Ballantyne (1993). All clast data were plotted using a modified version of the TriPlot program developed by Graham & Midgley (2000). Roundness was measured by assigning clasts to categories (very angular to well-rounded) using descriptive criteria (Benn & Ballantyne, 1993). For each sample, shape and roundness were summarised using the C_{40} index (percentage of clasts with a c:a ratio of ≤0.4), the RA index (percentage of very angular and angular clasts) and the RWR index (percentage of well-rounded and rounded clasts). These indices have proved to be a very powerful means of differentiating clast populations transported by active (subglacial), passive (englacial and supraglacial) and fluvial processes (e.g. Benn & Ballantyne, 1994; Benn, 2004; Lukas et al., 2013). Data were interpreted with reference to control samples from modern glacial environments (Hambrey & Glasser (2012). The control samples represent possible alternative transport domains, including active subglacial, passive supraglacial and glacifluvial, rather than particular topographic or climatic settings. To ensure that samples were taken from a single facies, they were necessarily of mixed lithology. Sampled clasts were predominantly intrabasinal sandstone, limestone and dolostone, with occasional far-travelled basement lithologies. Fissile lithologies such as shale were avoided. The use of mixed lithologies may reduce the discriminatory power of clast shape analysis, but with due caution useful results can still be obtained (Lukas et al., 2013).

Clast fabric analysis was performed by measuring a-axis orientations of samples of 50 clasts, following the recommendation of Ringrose & Benn (1997). Data were summarised using the

eigenvalue method of Mark (1973), which computes the orientation and strength of three orthogonal eigenvectors (V_1, V_2 and V_3; and S_1, S_2 and S_3, respectively). All data were rotated to remove the effect of bed dip. To aid interpretation of depositional and deformational processes, fabric shape was plotted on triangular diagrams following the methods of Benn (1994).

Structural analysis was undertaken in the field and during subsequent laboratory-based microscopic investigations of thin sections. In this study, the term *soft-sediment deformation* is used to distinguish rock that has been deformed through primary processes (for example, slumping and glacitectonism) from rock that has been deformed tectonically. Although it is acknowledged that some of this primary deformation is not necessary strictly 'soft' because some of the facies were well-lithified prior to deformation (see *Deformed rhythmite facies (B-1)* section).

Polished thin sections of deformed rhythmites were obtained from Andromedafjellet and Ditlovtoppen for micro-structural analysis. These were aligned parallel to the dominant ice-flow orientation where possible and were analysed using a standard petrographic microscope at low magnification, under plane-polarised and cross-polarised light.

The thin section study of micro-structures is commonplace in study of Quaternary glacial successions (e.g. van der Meer, 1993; Menzies, 2000; Carr, 2001). Despite this, several features including various rotational features are common to multiple settings, for example shearing debris flows and glacitectonites (e.g. Phillips et al., 2002; Busfield & Le Heron, 2013). Because subjectivity can be an issue during the analysis and interpretation of microstructures, particularly in massive diamictites, AMS was also employed as an objective means to quantify fabric trends.

Orientated samples for measurement of AMS were collected using a combination of field-drilling and block sampling. Anisotropy of magnetic susceptibility (AMS) was measured using an AGICO KLY-3 Kappabridge (AGICO; Advanced Geoscience Instruments Company, Brno, Czech Republic) operating at 875 Hz with a 300 A/m applied field at the University of Birmingham, UK and an AGICO MFK-1A

Kappabridge operating at 976 Hz with a 200 A/m applied field at New Mexico Highlands University, USA. The AMS data were analysed using standard statistical techniques (Jelínek, 1981), calculating the orientation and strength of the three orthogonal axes of the susceptibility ellipsoid. Data were summarised using standard indices such as mean susceptibility (K_{mean}), corrected anisotropy degree (P_j), lineation (L) and foliation (F) parameters and the shape parameter (T) (Jelínek, 1981). In addition, the K_1 vector distribution was analysed through the eigenvalue method of Mark (1973) and data were plotted on shape triangles (cf. Benn, 1994a). These diagrams facilitate the visualisation and interpretation of AMS fabrics in sedimentary rocks. It is recognised that the AMS data are not directly comparable to clast fabric data, because they are a function of both mineral magnetic properties and grain orientation. The AMS fabrics of the Wilsonbreen Formation typically reflect the preferential alignment of paramagnetic phyllosilicate clay minerals, with a minor contribution of multidomain (MD) titanomagnetite and fine-grained maghaemite in some cases (Fleming, 2014). A minor anomalous single domain (SD) ferromagnetic source was identified in some samples and these were omitted from subsequent analysis.

4. FACIES DESCRIPTIONS

Diamictite makes up over 80% of the Wilsonbreen Formation (Fig. 3). For the purposes of description, the diamictites and associated sediments are subdivided into Undeformed and Deformed Facies Associations.

4.1. Undeformed Facies Association

The Undeformed Facies Association occurs at all the studied outcrops, but is generally thicker in sections to the north. It can be subdivided into (A-1) diamictite facies and (A-2) sandstone and conglomerate facies (summarised in Table 1).

4.1.1 Diamictite facies (A-1)

The Undeformed diamictite (Dm and Ds) is typically greenish-grey or maroon, clast-poor, with a poorly sorted sandy matrix (Fig. 4A, B and D). Clasts make up between 3% and 10% of the facies, although clast-rich and sand-poor varieties occur and all proportions up to gravel may be present. The majority of clasts are intrabasinal (60 to 80%) and can be matched with underlying strata, particularly the Elbobreen and Backlundtoppen Formations (dolostone, limestone, chert, breccia and siltstone; Fairchild & Hambrey, 1984). The remainder are extrabasinal and some have an unknown source area. Of these, coarse-grained pink granite is most common, but other granite as well as basalt, banded gneiss, quartzite and amphibolite also occur. Clast size spans a wide range and boulders >80 cm are observed locally.

The sand fraction is composed predominantly of subangular quartz with minor dolostone, mica and other lithic fragments. Opaque minerals are common and are mostly composed of pyrite, haematite or magnetite; they often form separate, subangular to rounded grains which suggest a detrital origin. This is presumably derived from the weathering and erosion of the igneous and metamorphic lithologies; however, secondary growth of haematite and pyrite is seen in places. The silt fraction grades into a dolomicrite matrix with varying proportions of quartz and clay minerals. This is commonly obscured by a well-developed haematite staining, particularly pronounced in maroon diamictites.

Bedding is poorly developed and can usually only be seen where diamictites are interbedded with associated facies (for example, conglomerates and sandstones). Where it is seen, bed thickness ranges from 2 to 5 m. 'Wispy' stratification is seen in some cases (for example, Fig. 4A). This is normally defined by changes in the sand content of the diamictite matrix and is sometimes associated with colour change or mottling.

Clast-shape data are shown on Ternary shape diagrams and roundness histograms in Fig. 5A and B. Relatively low C_{40} indices indicating large proportions of 'blocky' as opposed to platy or elongate

clasts. In all sites, most of the clasts are subangular to subrounded, and very angular and well-rounded clasts are rare or absent. Covariance plots of RWR-C_{40} and RA-C_{40} for the diamictites are shown in Fig. 5C, together with data from modern control sites (Fig. 5D; Hambrey & Glasser, 2012). Clast shape is closely similar to samples from modern subglacial till, and differs from both passively and fluvially transported clasts from modern environments. A variety of surface textures occur on the clasts. Striations are common on the fine-grained lithologies, affecting up to 28% of the clasts, and are orientated randomly or form subparallel sets. Facets are common (affecting up to 50% of clasts). The textural data thus support the conclusion that the clasts underwent subglacial transport prior to deposition.

4.1.2 Sandstone and Conglomerate facies (A-2)

Pale yellow to greenish grey, moderately to well-sorted sandstones (Sm and Ss) are commonly interbedded with the diamictite, and form laterally continuous sheets or discontinuous lenses (for example, Fig. 4C). Bed thickness varies widely, from <10 cm to 1/2 m. In total, the sandstone facies make up 4 to 8% of the Wilsonbreen Formation (Fig. 3).

Grain size is mostly fine to medium sand but is highly variable. Quartz is the predominant grain lithology in the majority of cases (>95%), defining a quartz arenite, with minor feldspar, dolomite and other lithic fragments. Outsized clasts are common and are composed of the same lithologies as those contained in the surrounding diamictites. Opaque minerals are observed in thin section and are composed predominantly of subrounded grains of haematite and magnetite with local development of authigenic pyrite. Both silica and carbonate cements are observed, and quartz overgrowths are common at grain boundaries. A silty sand matrix with varying proportions of dolomicrite, clay minerals and quartz, sometimes obscured by haematite cement, is also seen in places. The proportion of this matrix relative to encompassing grains varies considerably from being almost absent up to near greywacke proportions.

Bedding geometry typically is either channel-like and lenticular (for example, Fig. 4C) or laterally extensive and planar. The contacts with overlying and underlying diamictites are mostly sharp. The channel-like sandstone beds display an erosive base that cuts into underlying diamictites. Occasionally, rippled tops are seen. Stratification is typically wavy and discontinuous where observed, but is chaotic in places. In addition, both trough and planar cross-stratification is locally developed, particularly in the sandstone beds displaying channel geometries.

Conglomerate interbeds (Gm and Gs) are also commonly associated with the diamictites (for example, Fig. 4E); these form either isolated lenses or continuous sheets up to 50 cm thick. The interbeds can be laterally extensive and remain fairly uniform in thicknesses, or they can be discontinuous and lenticular in form. Some show subtle reverse grading, whilst others have a sharp undulating base with evidence of erosion and channel forms. Normal grading into overlying massive diamictites is seen locally. The clast fraction (50 to 90%) is composed of similar lithologies to the diamictites. Grains are angular to rounded (predominantly subrounded), and sorting is poor to medium. The matrix is typically a medium to poorly sorted, fine to coarse sand, and is composed predominantly of angular quartz grains, sometimes surrounded by a muddy dolomicrite.

At both Dracoisen and Ditlovtoppen, there are high concentrations of sandstone and conglomerate beds in parts of the W3 Member (Fig. 3C and D). These are interbedded with diamictite beds and form tapering wedge-shaped structures apparently thinning to the north and dipping 10° more steeply than the regional bedding (Fig. 6). The sandstone and conglomerate beds in these areas are commonly affected by convolute bedding and slump structures, indicating local syn-depositional deformation.

4.2. Deformed Facies Association

The Deformed Facies Association (Fig. 7) occurs in W3 and W1 immediately above and below the W2 Member, respectively, at Reinsryggen, Ditlovtoppen and Andromedafjellet (Fig. 3). Possible other

examples occur at higher levels in W3 at the same sites, although exposure is generally too poor to allow detailed study. Deformed facies are absent from Dracoisen. The Deformed Facies Association can be subdivided into: (B-1) deformed rhythmites, (B-2) diamictites, (B-3) sandstones and conglomerates and (B-4) boulder pavements (Summarised in Table 2).

4.2.1 Deformed rhythmite facies (B-1)

Evidence for extensive disruption and deformation of rhythmites is seen at Ditlovtoppen and Andromedafjellet in the uppermost part of the W2 Member, at the boundary with the overlying W3 Member (Fig. 3B and C). The deformed rhythmites display extensive folding and faulting at both microscopic and macroscopic scales, but they otherwise compositionally and texturally correspond well to the undisturbed rhythmites of the underlying W2 Member facies. At Ditlovtoppen, a 2 m thick zone of deformed rhythmites is observed, which passes into overlying diamictites of the W3 Member (Fig. 7H). The deformed zone can be traced 200 m laterally along strike. Deformed rhythmites are also seen at Andromedafjellet in a 1 m thick zone located beneath massive maroon diamictites of the W3 Member. The rhythmites are composed of 2 to 10 mm silt/sand–carbonate couplets with a slightly greater sand fraction than those at Ditlovtoppen.

It is important to assess whether the deformation structures are primary, related to deposition mechanisms (for example, glaciotectonism or slumping), and not the result of subsequent tectonic overprinting. A tectonic origin for the deformation structures can be ruled out for several reasons. The deformation is localised and does not cross-cut formation boundaries. It occurs within distinct horizons where, based on sedimentary structures, a relationship to depositional processes can be demonstrated. Furthermore, the deformation is not dependent on lithology but varies stratigraphically through the section. For example, both deformed and undeformed rhythmite varieties occur at different stratigraphic levels. Finally, although the rocks have been folded into a syncline during the Caledonian Orogeny, pervasive tectonic deformation is absent at the study sites and there is no associated cleavage formation. The folding pattern is not consistent with the Caledonian trend. Instead, the folds are either chaotic or show dominant vergence to the north.

Deformation occurred in both ductile and brittle manners, the style of which appears, at least in part, to be controlled by sediment composition and texture. The carbonate fraction displays brittle deformation, whilst the silt-sand matrix is deformed in a ductile manner (for example, Fig. 8A and B). This appearance can be explained by early cementation of the carbonate horizon, prior to deformation, and water-saturation of the silt-sand matrix; this is also consistent with the occurrence of carbonate intraclasts in undeformed sediments. The brittle faults typically form conjugate pairs or appear chaotic, and they show no uniform pattern in shear in any particular direction. However, high-angle normal faults and low-angle reverse faults are identified in places. These display possible Riedel shear geometries (Riedel, 1929) that may highlight simple shearing. In addition, the presence of sand veins in between the faulted carbonate laminae suggests that the sand fraction was subject to liquefaction and remobilisation during folding.

There is typically an increase in the intensity of deformation up section, and the deformed rhythmites pass upward into massive diamictites (B-2). At the base of the deformed rhythmites, deformation is typically small-scale and is characterised by the occurrence of conjugate faults, showing both low-angle and high-angle reverse offset. Some display possible Riedel shear geometries (for example, Fig. 8C). The offset along faults is typically low (up to several centimetres). In addition, small-scale thrust-faults and augen-like structures are seen. The offset along conjugate brittle faults and thrusts increases upwards in the section towards the boundary with the diamictite. Larger-scale recumbent folds are seen on the 0.2 to 1.0 m scale (Fig. 7F, I and K). Smaller-scale parasitic folding is sometimes seen on fold limbs. Fold vergence is typically to the north, although precise measurement is typically not possible because of a lack of three-dimensional exposure. Larger scale thrusts are also observed showing displacement of 50 cm or more (Fig. 7G and J), with dips towards the south.

The boundary with the overlying diamictites is typically transitional. At the top of the deformed rhythmites, north-verging, low-angle reverse faults are observed (Fig. 7G and J), some showing

displacement over 1 m. At Ditlovtoppen (Fig. 9A), dolostone rafts occur at the boundary between the diamictites and the rhythmites, showing internal folding and faulting and brecciation. In places, overlying diamictites envelop 0.5 to 2.0 m lenses of deformed rhythmite (Fig. 7E).

Evidence of intense folding and faulting in the deformed rhythmite facies is also seen microscopically (Fig. 8), with both brittle and ductile deformation. As is the case at the macroscopic scale, deformation style is determined in part by composition. Rhythmite couplets composed of carbonate display brittle deformation, often breaking into fragments separated by faults (Fig. 8A and B). In contrast, the silt-sand component of the rhythmite behaved in a ductile manner as it is commonly folded and fills in the space between the carbonate layers. This is clearly seen in Fig. 8B where the rhythmite displays a close monocline structure. At a large scale, the bed appears to be folded; however, microscopic analysis reveals that the folding is partially facilitated through faulting. Brittle deformation has occurred within the carbonate lamellae which produces tabular fragments, whereas the silt-sand fraction has undergone predominantly ductile deformation.

Faulting within the deformed rhythmites appears chaotic in places (for example, Fig. 8A) and the analysis of fault kinematics is challenging. However, high-angle reverse faults and low-angle normal faults (Fig. 8D) dipping to the south are common; these are interpreted as P and R_2 Riedel shear geometries, associated with shear to the north. Low-angle thrusts are also present typically dipping to the south (Fig. 8A). In places at the boundaries between faulted carbonate laminae, a network of sand-filled veins can be observed microscopically (for example, Fig. 8B). Sand within these veins has the same composition as the silt-sand component of the rhythmite couplet, but typically contains less of the silt fraction. An increase in the amount of folding and faulting is seen up to the boundary with the overlying diamictite. Figure 8D shows a highly deformed rhythmite taken from close to this boundary at Andromedafjellet. Sand within the rhythmites displays an augen-like geometry with asymmetric tails suggesting shear to the north. On either side of this augen structure, a low-angle shear zone dipping to the north separates the augen from the surrounding sandy lamination.

4.2.2 Diamictite facies (B-2)

Massive diamictite (Dm) is widespread in the Deformed Facies Association, occurring immediately above and below the W2 Member at Reinsryggen, Andromedafjellet and Ditlovtoppen (Fig. 3). Similar facies are also seen higher in the succession at these sites. The Diamictite is similar both compositionally and texturally to that seen in the Undeformed Facies Association. It consists of a poorly sorted mixture of clasts (both intrabasinal and extrabasinal) in a matrix dominated by fine-medium quartz sand, with minor amounts of lithic particles. It has subtle textures and fabric characteristics not seen in the Undeformed Facies Association, but the key difference is the presence of deformed lenses and rafts of underlying units, and the close relationship with other deformed facies. For example, at Reinsryggen (Fig. 10) diamictites beneath a boulder pavement contain deformed lenses of sandstone and conglomerate bodies (for example, Fig. 10C and D). The surrounding diamictite displays a weak fabric that appears to envelop the lens structure. Wispy lamination is sometimes observed immediately surrounding the lenses, showing evidence of small-scale folding and faulting (Fig. 10C). The sandstone lenses themselves are massive or stratified. Where present, the stratification is commonly undulating and folded, and faulting is common, especially at the margins of the lenses.

Clast-matrix ratios and composition are variable, but both ratios and the proportion of extrabasinal clasts are typically higher than in the undeformed diamictite lithofacies. At Ditlovtoppen, for example, a granite-rich horizon occurs in diamictites at the base of the W3 Member with a clast-matrix ratio above 40%. The clasts consist predominantly of granule to pebble-sized, subangular to subrounded red granite. Immediately overlying deformed rhythmites of the W2 Member at the same section, diamictites contain subangular fragments of rhythmite and carbonate. Diamictites of the Deformed Facies Association commonly display a fissile weathering pattern and are almost exclusively maroon, although mottling occurs locally (for example, Fig. 7C and D); in other cases, the diamictites are massive.

Clast-shape data for the diamicties of the Deformed Facies Association are shown in Fig. 5. The data resemble those for the diamictites of the Undeformed Facies Association. The majority of the clasts are subangular to subrounded and very angular and well-rounded clasts are rare or absent. Comparison with control data indicates that the debris has undergone subglacial transport, a conclusion consistent with the abundance of striated and facetted clasts, particularly on the carbonate lithologies.

4.2.3 Sandstone and conglomerate facies (B-3)

Occurring within the diamictites are lenses of maroon and pale yellow-grey sandstone (Sm and Ss) and conglomerate bodies (Gs and Gm; Fig. 3). Lenses typically have a planar upper surface and concave-up lower surface, and are generally less than 2 m in lateral extent, but are locally up to 25 m wide (Fig. 10). The sandstone is predominantly medium-grained, but is locally much finer. In addition, conglomerates occur locally, either as isolated lenses or as dispersed clasts within sandstone lenses. Sandstones are typically poorly sorted and are dominated by subangular to subrounded grains of quartz, lithic fragments and opaque minerals in a fine-grained matrix of varying proportions (5 to 20%).

Contacts with surrounding diamictites are typically sharp, although a 5 cm thick reduced zone is seen occasionally within the maroon diamictite that envelops the lenses. The sandstone and conglomerate is either massive or displays subtle stratification (Fig. 10C), and is commonly folded and faulted. Some lenses appear less deformed and display subtle cross-lamination with rare climbing ripples (Fig. 10D). At Reinsryggen, small (2 to 4 m wide) deformed sandstone lenses are overlain by a large 10 m wide sandstone body (Fig. 10); this has a distinctive erosive base and is truncated top at the boundary with a nascent boulder pavement (Fig. 10A).

4.2.4 Boulder pavements (B-4)

Boulder pavements occur at two localities within the Wilsonbreen Formation. At Ditlovtoppen (Fig. 3C), a distinct boulder pavement, previously described by Chumakov (1968) and Fairchild & Hambrey (1984), is seen 2 m above the contact with deformed rhythmites of the W2 Member. It is composed of a boulder conglomerate with clast a-axes predominantly 10 to 20 cm, but up to 50 cm. Clast lithologies are mostly dolostone, but other intrabasinal and extrabasinal lithologies are present. The clasts sit in maroon sandy matrix that is composed of fine-grained, subangular quartz and lithics in a silty sand matrix. Clasts at the top surface of the pavement show a flat, planed-off top, on which unidirectional striations trend of 130°. Overlying the boulder pavement is a massive, maroon diamictite of the Deformed Facies Association (B-2). Twenty-five metres along strike, the boulder pavement changes to a granite-rich horizon with clast concentrations of over 30%.

A second boulder pavement occurs at Reinsryggen (Fig. 10), occurring 30 m above the contact with the W2 Member. In contrast to the boulder pavement at Ditlovtoppen, the clasts are matrix-supported and concentrations are distinctly lower (10%). The clasts are enclosed within a maroon sandy diamictite with a silty sand matrix. Forty metres along-strike to the north, the boulder pavement lies at the top of a 30 metre wide channelised maroon sandstone body composed of poorly-sorted, fine-grained subangular quartz grains. Clasts have a faceted top surface (Fig. 10B), but striations were not observed at this locality.

4.3. Clast and Anisotropy of Magnetic Susceptibility (AMS)Fabrics

Clast fabric data (Table 3) are shown on lower-hemisphere, equal-area stereographic projections (Fig. 11) and fabric shape triangles (Fig. 12). Nine of the samples are from diamictite of the Undeformed Facies Association at Dracoisen (1a), Ditlovtoppen and Andromedafjellet, and six from diamictite of the Deformed Facies (2b) at Ditlovtoppen (5) and Andromedafjellet (1). Four of the

Ditlovtoppen Deformed facies samples are from the near the base of W3, and the fifth from near its top. Fabrics from the two diamictite facies have contrasting characteristics, plotting in almost distinct fields on shape triangles (Fig. 12A). Fabrics from the Undeformed diamictites (1a) (Fig. 12A-i) are mostly girdles with insignificant to weak preferred orientations, whereas those from the Deformed diamictites (2b) (Fig. 12A-ii) are moderate to strong clusters. The latter are similar to fabrics from modern subglacial traction tills (e.g. Benn, 1994b, 1995), consistent with orientation of clasts by simple shear (Benn, 1995). Preferred orientations (V_1) of the deformed facies samples lie in the range 136° to 184° (Table 3). Although the fabrics from the undeformed facies (1a) are much weaker, their preferred orientations span a similar range (144° to 192°) with two outliers. It should be noted that vector azimuths are relative to modern True North, and do not take into account any net rotation of the Svalbard landmass since the Neoproterozoic.

Samples for AMS analysis were taken from sandstone and diamictite of the Undeformed Facies Association (1a), and diamictites and deformed rhythmites of the Deformed Facies Association (2b). Sandy diamictite was preferentially targeted as sampling of the muddy diamictites of the Undeformed Facies Association was problematic due to their friable nature. In most samples, the AMS is controlled by preferential alignment of paramagnetic phyllosilicate clay minerals (Fleming, 2013).

AMS results are shown in Table 4 and are plotted on to stereonets in Fig. 13. The distribution of the K_1 vector (Table 5) are analysed through shape triangles in Fig. 12. The magnetic anisotropy is typically low, mean values of the corrected degree of anisotropy P_j were close to one and showed no variation with depositional facies. These results follow the experimental results of Hooyer et al. (2008), where no correlation with between shear strain and the degree of anisotropy were observed. In these experiments, however, distinct correlation was found in the alignment of K_1 orientations with increasing shear strains, measured through the S_1 eigenvalues. Similarly in this study, distinct variation can be seen in the alignment of the K_1 axes with depositional facies,

visualised through the shape triangles (Fig. 12B). In these plots, there is an almost complete distinction between the fabric shape of samples from the Undeformed Facies Association (1a) (Fig. 12B-i) and Deformed Facies Associations (2b) (Fig. 12B-ii and B-iii). The samples from the Undeformed Facies Association (1a) are moderately to strongly elongate (E = 0.38 to 0.89), with the azimuth of the K_1 axes spanning a very broad range. In contrast, five of the six samples from diamictites of the Deformed Facies Association (2b), and three of the four samples from the deformed rhythmites (2a) are very strongly elongate (E = 0.90 to 0.98). The K_1 axis azimuths of the deformed facies diamictite samples lie in the range 154° to 190°, similar to the V_1 orientations of the clast fabrics. Two of the K_1 axis azimuths for the deformed rhythmites are similar, and a third lies at 180° to the main trend.

Variation in azimuth of the mean K_1 axes is seen within the stratigraphic section at some sites (Fig. 13). For example, at Ditlovtoppen there is a possible switch in fabric orientation up-section. AMS fabrics at the base of the W3 Member typically lie in a north–south orientation, whilst higher in the sequence a shift is seen to predominantly north-west/south-east orientated K_1 azimuths. In spite of this local variation, the dominant fabric trend lies in a north-south orientation at all sections.

5. LITHOFACIES INTERPRETATION

5.1. Undeformed Facies Association

5.1.1 Diamictite

The presence of subtle stratification, the close association with facies typical of subaqueous deposition and a lack of associated subglacial facies (for example, boulder pavements and glacitectonic deformation) suggest that deposition of the diamictites of the Undeformed Facies Association occurred mainly in a subaqueous glacial environment. The occurrence of faceted and

striated clasts indicates that, prior to deposition, the debris underwent subglacial transport below warm-based ice (e.g. Boulton, 1978).

In subaqueous environments, thick structureless diamictites can form by release of sediment from a high concentration of debris-rich icebergs (e.g. Dowdeswell et al., 1994; Syvitski et al., 1996), close to a grounding line. The subtle stratification can be interpreted as the product of minor subaqueous current reworking and subsequent removal of fines during rainout deposition of diamictite from floating ice.

The girdle clast fabrics from the diamictites are consistent with a dropstone origin (Domack & Lawson, 1985). Weak preferred orientations can develop in response to bottom currents or reorientation by mass flow. The preferred orientations (V_1) of these samples suggest persistent bottom currents or mass flow along a north-south axis.

5.1.2 Sandstone and conglomerate facies

Channelised sandstones (Fig. 4C) are a common feature of glacially influenced subaqueous environments (e.g. Le Heron et al., 2013) and are particularly associated with the influx of sorted sands from subglacial channels emerging at the grounding line (Powell, 1990). The conglomerate facies is interpreted as either mass flow deposits or erosional lags. Lags can form in subaqueous environments during periods of non-deposition or times of increased bottom water-flow. In these situations, finer material is removed by bottom water currents (e.g. Powell, 1984). Conglomerates displaying reverse grading and sharp contacts with overlying diamictites are interpreted as lags. In contrast, those that have lenticular or channel-like geometries and display normal grading are interpreted as mass flows. These are common in both glacimarine and glacilacustrine environments where deposition occurs on a slope steep enough to facilitate failure (Laberg & Vorren, 1995; Eyles & Eyles, 2000; Hambrey & McKelvey, 2000). Such slopes can be readily created in glacial environments, particularly in the proximal zone close to the grounding line (Powell, 1990). Here, the emergence of sediment-laden water from subglacial tunnels results in high rates of deposition. As such, local

topographic highs and associated slopes develop at the grounding line. In these settings, sediment remobilisation events, such as debris flows, occur in tectonically quiescent basins where the bathymetry is otherwise flat.

The distinctive architecture of tapering beds of diamictite, sandstone and conglomerate sloping at 10° to the upper and lower bounding surfaces is characteristic of proximal grounding-line fans (Fig. 6). The associated sandstone and conglomerate debris flow deposits are interpreted as episodic sediment pulses delivered from the subglacial drainage system. Convolute bedding and slump structures record local failure of these sediments. The Interbedded massive diamictites are interpreted as rainout deposition from suspended sediment, combined with background sedimentation from icebergs.

The AMS fabrics from the sandstone and conglomerate facies (Fig. 13) are consistent with particle orientation by shearing in cohesionless flows, with relatively low cumulative strains (Hooyer et al., 2008). Taken together with the geometry of the grounding-line fan deposits, K_1 azimuths suggest sediment transport in a broad arc towards the north or north-west.

Non-glacial lacustrine, evaporite, fluvial and periglacial sediments occur at several levels within the Wilsonbreen Formation, and the basin appears to have been isolated from the sea throughout (Benn et al., 2015; Fairchild et al., this issue). The present authors therefore interpret the Undeformed Facies Association as glacilacustrine, deposited in a large proglacial lake. At times, deposition occurred in an ice-proximal setting close to the glacier grounding-line, but at other times deposition was dominated by rain-out in a more distal environment. The occurrence of carbonate lacustrine facies with dropstones in the W2 Member (Fairchild et al., this issue) indicates that periodic input of glacial sediment to the lake was much reduced. The massive diamictites formed by a combination of rainout from a high concentration of debris-rich icebergs and the settling of material from meltwater plumes. High rates of sedimentation resulted in the development of local palaeoslopes and the formation of grounding-line fans (Fig. 6). Sediment remobilisation events resulted in the

emplacement of debris flow deposits. In addition, subaqueous currents, possibly created by emerging subglacial channels, formed lag deposits.

5.2. Deformed Facies Association

5.2.1 Origin of the deformed rhythmites and overlying diamictite

On the basis of their structural style and close association with sheared diamictites, the deformed rhythmites are interpreted as glacitectonite (cf. Benn & Evans, 1996; Benn & Evans, 2010). Prior to deformation, these rhythmites were originally both structurally and compositionally similar to the rhythmites of the undeformed W2 Member (Fairchild et al., this issue). The original deposition of the unit occurred in a lacustrine environment with the lamination reflecting daily, meteorological or annual variations in sediment discharge into a lake. The deformation of the rhythmite records glacier advance over the site. Evidence for partial liquefaction and local upward injection of sediments suggests hydrofracturing, which is a common feature of subglacially deformed sediments (Phillips et al., 2013).

The diamictites that overlie these deformed rhythmites are interpreted as subglacial traction tills (Benn & Evans, 2010). The tills formed partially by the deformation of the immediately underlying sediments (recorded by the presence of rafts of lacustrine carbonates, glacitectonite and other deposits) and partially by the transport of intra- and extra-basinal debris from upglacier. The clast fabrics from the diamictite and the AMS fabrics from the diamictite and the glacitectonites are consistent with particle orientation by shearing, with high cumulative strains (Benn, 1994a, 1995; Iverson et al., 2008). The transitional contacts between the rhythmites and the overlying diamictites and consistent fabric orientations suggest that the deposition of both deposits occurred during the same glacial advance, with ice movement from the south or south-south-east.

5.2.2 Origin of sandstone and conglomerate lenses within diamictites

Lenses of sand and gravel within massive diamicton are a common feature of subglacial traction tills (e.g. Hart & Roberts, 1994; Evans & Campbell, 1995). A variety of mechanisms has been proposed for their formation (see review in Waller et al., 2011), including entrainment of the sand through thrusting or folding from an underlying layer (e.g. Hart & Boulton, 1991), and the melt-out of sand from the overlying basal ice (e.g. Hoffmann & Piotrowski, 2001). Alternatively, sands and gravels may be produced subglacially by the deposition of sorted sediments flowing within subglacial channels at the ice-bed interface (Alley, 1991; Clark & Walder, 1994). Although being originally fluvial in origin, these deposits can be cannibalised and deformed by the array of processes associated with the formation of a subglacial traction till (Hart, 1998; Evans et al., 2006; Benn & Evans, 2010), and they are subsequently incorporated as deformed lenses in otherwise massive diamicton.

Within the sandstone lenses of the Deformed Facies Association, a mechanism through thrusting of pre-existing sands is unlikely owing to the lack of similar sands lower down in the sequence. Furthermore, the identification of channel-like geometries on some of the lenses with deformed cross-bedding is consistent with a glacifluvial origin. For example, the large channelised sandstone body occurring immediately below the boulder pavement at Reinsryggen (Fig. 10A) has a geometry typical of a subglacial channel. Therefore, the sandstone and conglomerate lenses of the Deformed Facies Association are interpreted as subglacial channels, some of which have been deformed and incorporated into a subglacial traction till, whilst others remain undeformed such that their depositional geometries are preserved.

5.2.3 Development of the boulder pavements

Striated Boulder pavements are considered diagnostic of subglacial environments (e.g. Boyce & Eyles, 2000) . A boulder pavement in a till succession consists of a thin, laterally extensive layer of clasts, commonly with planar and sometimes striated upper surfaces. A number of different mechanisms have been proposed for their formation. The most straightforward suggestion is that

they represent the former position of the ice-bed interface, where the combined effects of subglacial meltwater and glacier sliding progressively remove fine-grained sediment from the underlying till, leading to a concentration of larger clasts (Boyce & Eyles, 2000). However, Clark (1991) and Boulton (1996) suggested that pavements could also form within the deforming bed itself, as a result of clasts sinking through soft sediment or excavation at the base of the deforming layer.

The boulder pavements at Ditlovtoppen and Reinsryggen represent very prominent surfaces that can be traced for several hundred metres along strike; they possibly mark periods of distinctive subglacial conditions, when erosional and deformational processes dominated over depositional ones within the deforming bed mosaic. Although the Ditlovtoppen and Reinsryggen pavements occur at a similar stratigraphic level, it is not known whether they are precisely synchronous, or represent diachronous shifting of subglacial environments in different areas.

At both Ditlovtoppen and Reinsryggen, sand-filled channels occur in association with the boulder pavements, incised down into the underlying diamictite and with planar tops level with the boulder pavement surfaces. These channel structures are significant because they indicate the presence of meltwater at ice-bed interface.

At Ditlovtoppen, striations on the upper surface of clasts in the pavement are orientated to 130°; this is almost parallel to the V_1 eigenvector from a clast fabric (136°) and the K_1 vector of an AMS fabric (139°) from the underlying diamictite. This indicates that the boulder pavement and the underlying diamictite were formed while ice was flowing in a consistent direction.

Boulder pavements are a distinctive feature in subglacial sediments. Importantly for Neoproterozoic palaeoclimatic interpretations, the occurrence of boulder pavements and associated subglacial channel deposits clearly indicate a warm-based thermal regime for at least part of the depositional phase, with abundant water at the ice-bed interface.

6. DISCUSSION

The present study has obtained the first results from the application of anisotropy of magnetic susceptibility (AMS) to Neoproterozoic diamictites for sedimentological analysis. The use of AMS in combination with facies analysis, microstructural analysis and more traditional clast fabric analysis has enabled the depositional regimes of the Wilsonbreen Formation to be elucidated. In particular, AMS has allowed the kinematics of deformation to be constrained in an much more objective manner than was previously possible. It has also allowed the interrogation of parts of the section where structures are missing. Finally, it has allowed the analysis of fabric at a smaller and more precise scale than could be obtained through clast macrofabric analysis alone. These results suggest that, in addition to modern and Quaternary glacial sediments, AMS can be used as an effective petrofabric indicator in pre-Quaternary glacial sediments. This technique could be particularly useful where clast fabrics cannot be measured (for example, where they are too indurated to allow extraction of clasts).

The fabric data presented provides insight into palaeoflow during deposition. Fabric maxima in both the clast fabrics and AMS ellipsoids trend north–south in both the glacilacustrine and subglacial facies. In the glacilacustrine deposits, this probably reflects the direction of bottom currents and mass flows, whereas in the tills and glacitectonite, the (stronger) fabric maxima reflects the direction of shear beneath the glacier.

Iverson et al. (2008) showed that during subglacial shear of till, AMS fabrics develop with an up-glacier dip of K_1. The same up-glacier dip has been noted in the V_1 direction of clast fabrics from deformation tills (e.g. Benn, 1995). A slight predominance of dips towards the south is seen in the K_1 AMS and V_1 clast fabrics of the Deformational Facies Association, which could be considered consistent with shear towards the north. Both structural analysis of the glacitectonites and larger-scale sediment architecture supports the interpretation of ice flow and sediment transport to the north. Subglacial tills, indicative of grounded ice, are absent from the northernmost section

(Dracoisen). At this latter site, a grounding-line fan occurs at the same stratigraphic level, with beds tapering and dipping towards the north (Fig. 6). Thus, it is concluded that the glacigenic facies in the Wilsonbreen Formation were formed in association with a lobe of ice flowing into a large lake from the south. This conclusion is consistent with previous reconstructions of the palaeoenvironment (Fairchild & Hambrey, 1984; Halverson et al., 2004), and from the contiguous sediments of Northeast Greenland (Moncrieff & Hambrey, 1988; Herrington & Fairchild, 1989).

The extent of the outcrop of the Wilsonbreen Formation (and its correlatives in Northeast Greenland), and the wide range of both intrabasinal and extrabasinal clasts in the diamictites, suggests that deposition occurred in association with a large, possibly continental-scale ice sheet. The total thickness of the diamictite beds in the Wilsonbreen Formation (>100 m at most sites) implies a high sediment flux. Sediment was delivered into the lake by both glacial meltwater and calved icebergs, forming grounding line fans and thick rainout diamictites. The Deformed Facies Association provides abundant evidence of warm-based subglacial conditions, in the form of striated and polished clasts with compact 'blocky' shapes, sheared subglacial traction tills and glacitectonites, striated boulder pavements and subglacial channel deposits. Therefore, it is clear that in the area of outcrop (and, by implication, upstream) the ice was warm-based during the deposition of the preserved sediments. Warm ice occurs beneath many thick glaciers and ice streams even in modern polar environments, where the bulk of the ice is below the pressure melting point. The lack of facies with supraglacial attributes, and only a small proportion of fluvial sediment, is consistent with low topography and the presence of an ice stream, feeding into the lacustrine basin.

This study has focused on one particular part of the succession and has shown evidence of a major ice advance. However, this advance was not the only advance recorded in the Wilsonbreen Formation, because both glacilacustrine and subglacial sediments are interbedded with non-glacigenic facies in other parts of the succession (see Fig.1; Fairchild et al., this issue; Benn et al., 2015). The interplay of glaciolacustrine, subglacial and non-glacial conditions indicates that the

Marinoan glaciation in north-east Svalbard was characterised by repeated advance and retreat cycles. Model results and geochemical analyses presented by Benn et al. (2015) indicate that these cycles are likely to have occurred in response to orbital forcing in the late stages of the panglaciation. The evidence presented in the current paper for warm-based ice, subglacial fluvial systems, and thick glacilacustrine deposits shows that, for at least part of the Marinoan glaciation, glacier systems were dynamic and subject to repeated major changes.

7. CONCLUSIONS

Detailed investigations of the Wilsonbreen Formation have been undertaken utilising facies analysis, structural geology and fabric analyses. The following conclusions can be drawn:

- Deposition of the Wilsonbreen Formation occurred in subaqueous, subglacial and terrestrial settings, with advances of glacier ice along the axis of the basin. Glacigenic sediments were deposited in a predominantly subaqueous environment in the north and alternating subglacial and subaqueous environments in the south.
- A range of soft-sediment deformational structures occur within the Wilsonbreen Formation. Through detailed sedimentological and structural analysis, these are shown to be primary in origin, relating to deformation and deposition in a subglacial environment.
- This study has built on the previous work of the examination of anisotropy of magnetic susceptibility (AMS) of glacial sediments and shows that AMS in combination with clast fabric and facies analysis has the potential to provide significant insights into the deposition of well-preserved Neoproterozoic glacial sediments.

- Both Clast and AMS fabrics are found to exhibit consistent differences in shape and strength depending on the depositional mechanism. Subglacial tills and glacitectonites have very strong, elongate cluster fabrics parallel to the direction of shear. In contrast, clast fabrics from glacilacustrine diamictites are typically girdles, with weak preferred orientations possibly reflecting bottom currents or sediment flow. Anisotropy of magnetic susceptibility (AMS) fabrics from subaqueous mass flow deposits have moderate to strong preferred orientations through a broader range of orientations.
- In combination with analysis of the sediment architecture, the AMS and clast fabric data support the overall sedimentary architecture and indicate ice-flow to the north and continued northward sediment transport into a proglacial lake.

8. ACKNOWLEDGEMENTS

This work forms part of the NERC-funded GAINS (Glacial Activity in Neoproterozoic Svalbard) grant (NE/H004963/1) with a tied PhD studentship held by EJF. We would like to thank the logistical staff at UNIS for their help in the planning of the fieldwork. Finally, we would like to thank the reviewers, Flavia Girard and anonymous, and the associate editor (Dan Le Heron), for their comments and suggestions, which have considerably improved the manuscript.

9. FIGURE CAPTIONS:

Fig. 1 – Stratigraphic summary of facies within the Wilsonbreen Formation of north-east Svalbard with a location map of the study area showing the main exposures of the Wilsonbreen Formation. Red box denotes the area of focus in this study. DRA, Dracoisen; DIT, Ditlovtoppen; AND, Andromedafjellet; REIN, Reinsryggen; KLO, Klofjellet; McD, MacDonaldryggen; BAC, Backlundtoppen; PIN, Pinnsvinfjellet; ORM, Ormen; SLA, Slangen.

Fig. 2 – Summary of the Cryogenian stratigraphy of north-east Svalbard with the stratigraphic interval of focus in this paper shown in red (Wilson & Harland, 1964; Hambrey, 1982; Fairchild & Hambrey, 1984; Fairchild et al., 1989). Complete logs of the Wilsonbreen Formation in all sections are shown at in the supplementary information.

Fig. 3 - Detailed sedimentary logs with lithofacies interpretation of the W1–W2–W3 Member transition for: (A) Reinsryggen; (B) Andromedafjellet; (C) Ditlovtoppen; and (D) Dracoisen. Height refers to stratigraphic distance from the base of the formation.

Fig. 4 – Field photographs of the typical sediments associated with subaqueous facies associations of the W3 Member. (A) Clast-poor muddy diamictite horizon from Reinsryggen, displaying wispy undulating sand-rich lamination. (B) Massive maroon, clast-poor intermediate diamictite from Dracoisen showing a patch of clast-rich diamicton. (C) Channelised sandstone grey sandstone body cut into massive diamictite from Reinsryggen. (D) Massive friable, maroon, clast-rich sandy diamictite from Dracoisen. (E) Lenticular conglomerate (mass flow deposit) within massive diamictites forming part of the grounding-line fan at Dracoisen.

Fig. 5 – Clast morphological data. (A) Visual representation of triangular diagrams showing blocky, platy and elongate end members (after Benn & Ballantyne, 1993). (B) Data for clast-shape (triangular diagrams) and roundness (histograms) from massive diamictites from the Wilsonbreen Formation. (C) Covariance plots for all data from the Wilsonbreen Formation and (D) Modern control sites for comparison (after Hambrey & Glasser, 2012) showing variation in RA vs. C_{40}-index from polythermal glaciers in Svalbard (Midre Lovénbreen, Austre Lovénbreen and Austre Brøggerbreen).

Fig. 6 – The grounding-line fan at Dracoisen. (A) Field photograph of grounding-line fan. (B) Interpretative sketch of grounding-line fan rotated to horizontal showing inclined debris flow and diamictite beds in the W3 Member.

Fig. 7 – Field photographs of the typical sediments associated with the Deformational Facies Association: (A) is from Reinsryggen, (B) to (K) are from Ditlovtoppen and (L) is from Andromedafjellet. (A) Clast of black limestone from a massive diamictite bed showing a faceted, polished surface with several sets of striations. (B) Boulder pavement showing a large faceted granite clast overlain by mottled, friable diamictite. (C) Subglacial diamictite showing large, faceted dolostone clast within a massive diamictite bed with a fold picked out by mottling, overlain by massive diamictite. (D) Subglacial diamictite beds with horizon displaying mottling in sheared horizons. (E) Deformed rafts rhythmite from the W2 Member within massive friable diamictite (photograph: Douglas Benn). (F) Inclined fold at the top of deformed rhythmites displaying brecciation of individual carbonate lamina. (G) Glacitectonic thrust at the W2/W3 Member transition, showing partial raft formation. (H) Folded and faulted rhythmite overlain by friable diamictites of the W3 Member. (I) Recumbent fold with rhythmites with smaller-scale parasitic folds. (J) Glacitectonic thrust-fault within deformed rhythmites. (K) Isoclinal recumbent folding with maroon rhythmites. (L) Steeply dipping normal faults causing displacement of a 2 cm carbonate lamina within deformed rhythmites.

Fig. 8 – Microstructural analysis of deformed rhythmites. (A) Recumbent fold structure in faulted rhythmites, Ditlovtoppen. (B) Recumbent fold within deformed rhythmite at Ditlovtoppen showing brittle deformation and brecciation of carbonate horizons and ductile flow of sand–silt horizons, with sand-filled veins interpreted as hydrofractures cutting brecciated carbonate horizons. (C) Conjugate faulting in deformed rhythmites from Andromedafjellet. (D) Intense deformation from rhythmites at the boundary with overlying diamictite from Andromedafjellet displaying augen-like silty sand lens cut by low-angle shear zones.

Fig. 9 – Interpretative sketches of macroscopic deformational structures at the W2/W3 Member transition. (A) Deformed rhythmite showing conjugate, brittle faulting becoming progressively brecciated and disrupted towards the top, overlain by a deformed dolostone raft with internal

faulting and brecciation that passes into a subglacial diamictite. (B) South-verging thrust-fault with pop-up structures within a mottled silt/sand–carbonate rhythmite. (C) Extensive brittle and ductile deformation of rhythmites dominated by north-dipping, low-angle normal faults.

Fig. 10 – Interpretative sketch and photographs of the Deformed Facies Association at Andromedafjellet. (A) Field photograph and subsequent interpretative sketch displaying a boulder pavement overlying a subglacial diamictite (B-2) with lenticular sands and channel structures (B-3). Also shown are the AMS and fabric data obtained from the exposure (See Fig. 13 for Key), corrected for the tectonic dip. (B) Faceted granite clast at the top of a clast-poor boulder pavement (B-4), overlain by massive maroon diamictite. (C) Conjugate faulting and folding of wispy lamination surrounding a sandstone lens (B-3). (D) Sandstone lens with displaying disrupted, overturned cross-stratification (B-3).

Fig. 11 – Clast A axis orientation plotted on to equal area stereonets from (A) Dracoisen, (B) Ditlovtoppen and (C) Andromedafjellet (See Table 3 for data). All plots are corrected for tectonic dip. Facies codes in brackets where A-1 = Undeformed Facies Association, B-2 = Deformed Facies Association and U = Unknown.

Fig. 12 – Fabric shape diagram showing a continuum between isotropic, girdle and cluster fabrics, in which the eigenvalues (V_1, V_2 and V_3) are depicted as the axes of ellipsoids, the lengths of which are proportional to S_1, S_2 and S_3. (A) Clast fabric data from undeformed diamictites (i) and deformed diamictites (ii). (B) AMS fabric data, calculated using the eigenvalues of the K_1 axes from (i) undeformed diamictites, (ii) deformed diamictites and (iii) glacitectonite. See Tables 3, 4 and 5 for the data.

Fig. 13 – AMS orientation data showing the maximum (K_1), intermediate (K_2) and minimum (K_3) axes of the susceptibility ellipsoid from all subsamples, plotted on to equal area, lower hemisphere

stereonets from (A) Dracoisen, (B) Ditlovtoppen and (C) Andromedafjellet. See Tables 4 and 5 for the data

Fig. 14 – Summary diagram showing the Deformational Facies Association referred to in Table 2: (2a) glacitectonised rhythmites, (2b) subglacial diamictite with rhythmite rafts, (2c) subglacial diamictite with deformed lenses of sandstone and conglomerate (subglacial channel deposits) and (2d) a striated boulder pavement.

Table 1 – Summary of the lithofacies that make up the Undeformed Facies Association of W3.

Table 2 – Summary of the lithofacies that make up the Deformed Facies Association.

Table 3 – Data table of clast fabrics analysed using the eigenvalue method (Mark, 1973) where the data is resolved into three mutually orthogonal eigenvectors (V_1, V_2 and V_3). The shape and strength of the fabric is represented by the Eigenvalues S_1, S_2 and S_3. FA = facies association where A = Undeformed Facies Association, B = Deformed Facies Association and U = Unknown.

Table 4 - Mean site AMS data. No = number of samples; Km = mean susceptibility; K_1, K_2, K_3 = orientations (trend and plunge) of the principal susceptibility axes with 95% confidence ellipses; L = lineation ($L = K_1/K_2$); F = foliation ($F= k_2/k_3$); P_j = corrected degree of anisotropy; T = shape parameter; Fabric = whether the fabric can be classified as 'normal' (K_3 perpendicular, K_1/K_2 parallel to the bedding plane), 'inverse' (K_1 perpendicular and K_2/K_3 parallel to the bedding plane) or anomalous (K_1/K_2 deviation by >25° from bedding). FA = facies association where A = Undeformed Facies Association, B = Deformed Facies Association and B1 = glaciotectonite.

Table 5 – Anisotropy of magnetic susceptibility (AMS) orientation data analysed using the eigenvalue method (Mark, 1973) where the K_1 data is resolved into three mutually orthogonal eigenvectors (V_1, V_2 and V_3). The shape and strength of the fabric is represented by the Eigenvalues S_1, S_2 and S_3. FA = facies association where A = Undeformed Facies Association, B = Deformed Facies Association and B1 = glaciotectonite.

10. REFERENCES

Aber, J.S. and Ber, A. (2007) *Glaciotectonism*. Elsevier Science.
Alley, R.B. (1991) Deforming-bed origin for southern Laurentide till sheets? *Journal of Glaciology*, **37,** 125.
Benn, D.I. (1994) Fabric shape and the interpretation of sedimentary fabric data. *Journal of Sedimentary Research*, **64,** 910-915.
Benn, D.I. (1995) Fabric signature of subglacial till deformation, Breidamerkurjökull, Iceland. *Sedimentology*, **42,** 735-747.
Benn, D.I. (2004) Clast Morphology In: *A practical guide to the study of glacial sediments* (Eds D.J.A. Evans and D.I. Benn), pp. 77-92. Arnold London, London.
Benn, D.I. and Ballantyne, C.K. (1993) The description and representation of particle shape. *Earth Surface Processes and Landforms*, **18,** 665-672.
Benn, D.I. and Ballantyne, C.K. (1994) Reconstructing the transport history of glacigenic sediments: a new approach based on the co-variance of clast form indices. *Sedimentary Geology*, **91,** 215-227.
Benn, D.I. and Evans, D.J.A. (1996) The interpretation and classification of subglacially-deformed materials. *Quaternary Science Reviews*, **15,** 23-52.
Benn, D.I. and Evans, D.J.A. (2010) *Glaciers and glaciation*. Hodder Education, 816 pp.
Benn, D.I., Le Hir, G., Bao, H., Donnadieu, Y., Dumas, C., Fleming, E.J., Hambrey, M.J., McMillan, E.A., Petronis, M.S., Ramstein, G., Stevenson, C.T.E., Wynn, P.M. and Fairchild, I.J. (2015) Orbitally forced ice sheet fluctuations during the Marinoan Snowball Earth glaciation. *Nature Geosci*, **8,** 704-707.
Benn, D.I. and Prave, A.R. (2006) Subglacial and proglacial glacitectonic deformation in the Neoproterozoic Port Askaig Formation, Scotland. *Geomorphology*, **75,** 266-280.
Boulton, G.S. (1978) Boulder shapes and grain-size distributions of debris as indicators of transport paths through a glacier and till genesis. *Sedimentology*, **25,** 773-799.
Boyce, J.I. and Eyles, N. (2000) Architectural element analysis applied to glacial deposits: Internal geometry of a late Pleistocene till sheet, Ontario, Canada. *Geological Society of America Bulletin*, **112,** 98-118.
Busfield, M.E. and Le Heron, D.P. (2013) Glacitectonic deformation in the Chuos Formation of northern Namibia: implications for Neoproterozoic ice dynamics. *Proceedings of the Geologists' Association*, **124,** 778-789.
Carr, S. (2001) Micromorphological criteria for discriminating subglacial and glacimarine sediments: evidence from a contemporary tidewater glacier, Spitsbergen. *Quaternary International*, **86,** 71-79.
Chumakov, N.M. (1968) Okharaktere pozdnedokembriyskogo oledeneniya Shpitsbergena. [On the character of the Late Precambrian glaciation of Spitsbergen.] *Doklady An SSSR, Seriya geologicheskaya*, **180,** 1446-9.
Clark, P.U. and Walder, J.S. (1994) Subglacial drainage, eskers, and deforming beds beneath the Laurentide and Eurasian ice sheets. *Geological Society of America Bulletin*, **106,** 304-314.
Dowdeswell, J.A., Hambrey, M.J. and Ruitang, W. (1985) A comparison of clast fabric and shape in Late Precambrian and modern glacigenic sediments. *Journal of Sedimentary Research*, **55,** 691-704.
Dowdeswell, J.A., Whittington, R.J. and Marienfeld, P. (1994) The origin of massive diamicton facies by iceberg rafting and scouring, Scoresby Sund, East Greenland. *Sedimentology*, **41,** 21-35.
Evans, D.J.A. (2005) *Glacial Landsystems*. Hodder Arnold, 532 pp.
Evans, D.J.A. and Campbell, I.A. (1995) Quaternary stratigraphy of the buried valleys of the lower Red Deer River, Alberta, Canada. *Journal of Quaternary Science*, **10,** 123-148.
Evans, D.J.A., Phillips, E.R., Hiemstra, J.F. and Auton, C.A. (2006) Subglacial till: formation, sedimentary characteristics and classification. *Earth-Science Reviews*, **78,** 115-176.
Eyles, C.H. and Eyles, N. (2000) Subaqueous mass flow origin for Lower Permian diamictites and associated facies of the Grant Group, Barbwire Terrace, Canning Basin, Western Australia. *Sedimentology*, **47,** 343-356.

Eyles, N., Day, T.E. and Gavican, A. (1987) Depositional controls on the magnetic characteristics of lodgement tills and other glacial diamict facies. *Canadian Journal of Earth Sciences*, **34,** 2436–2458.
Eyles, N., Eyles, C.H. and Miall, A.D. (1983) Lithofacies types and vertical profile models; an alternative approach to the description and environmental interpretation of glacial diamict and diamictite sequences. *Sedimentology*, **30,** 393-410.
Eyles, N. and Januszczak, N. (2004) Zipper-rift': a tectonic model for Neoproterozoic glaciations during the breakup of Rodinia after 750 Ma. *Earth-Science Reviews*, **65,** 1-73.
Fairchild, I.J. (1983) Effects of glacial transport and neomorphism on Precambrian dolomite crystal sizes. *Nature*, **304,** 714-716.
Fairchild, I.J., Fleming, E.J.F., Bao, H., Benn, D.I., Dublyansky, Y.V., Halverson, G.P., Hambrey, J.M., Hendy, C., McMillan, E.A., Spotl, C., Stevenson, C.T.E. and Wynn, P.M. (In revision) Continental carbonate facies of a Neoproterozoic panglaciation, NE Svalbard. *Sedimentology*
Fairchild, I.J. and Hambrey, M.J. (1984) The Vendian succession of northeastern Spitsbergen: Petrogenesis of a dolomite-tillite association. *Precambrian Research*, **26,** 111-167.
Fairchild, I.J. and Hambrey, M.J. (1995) Vendian basin evolution in East Greenland and NE Svalbard. *Precambrian Research*, **73,** 217-233.
Fairchild, I.J., Hambrey, M.J., Spiro, B. and Jefferson, T.H. (1989) Late Proterozoic glacial carbonates in northeast Spitsbergen: new insights into the carbonate–tillite association. *Geological Magazine*, **126,** 469-490.
Fleming, E.J., Lovell, H., Stevenson, C.T.E., Petronis, M.S., Benn, D.I., Hambrey, M.J. and Fairchild, I.J. (2013a) Magnetic fabrics in the basal ice of a surge-type glacier. *Journal of Geophysical Research: Earth Surface***,** 2013JF002798.
Fleming, E.J., Stevenson, C.T.E. and Petronis, M.S. (2013b) New insights into the deformation of a Middle Pleistocene glaciotectonised sequence in Norfolk, England through magnetic and structural analysis. *Proceedings of the Geologists' Association*, **124,** 834-854.
Fleming, E.J.F. (2014) *Magnetic, structural and sedimentological analysis of glacial sediments: insights from modern, Quaternary and Neoproterozoic environments*, University of Birmingham, Birmingham.
Fuller, M.D. (1962) A magnetic fabric in till. *Geological Magazine*, **99,** 233-237.
Gentoso, M.J., Evenson, E.B., Kodama, K.P., Iverson, N.R., Alley, R.B., Berti, C. and Kozlowski, A. (2012) Exploring till bed kinematics using AMS magnetic fabrics and pebble fabrics: the Weedsport drumlin field, New York State, USA. *Boreas*, **41,** 31-41.
Graham, D.J. and Midgley, N.G. (2000) Graphical representation of particle shape using triangular diagrams: an Excel spreadsheet method. *Earth Surface Processes and Landforms*, **25,** 1473-1477.
Halverson, G.P., Maloof, A.C. and Hoffman, P.F. (2004) The Marinoan glaciation (Neoproterozoic) in northeast Svalbard. *Basin Research*, **16,** 297-324.
Halverson, G.P., Maloof, A.C., Schrag, D.P., Dudás, F.Ö. and Hurtgen, M. (2007) Stratigraphy and geochemistry of a ca 800 Ma negative carbon isotope interval in northeastern Svalbard. *Chemical Geology*, **237,** 5-27.
Hambrey, M. (1992) Secrets of a tropical ice age. *New Scientist*, **133,** 42-49.
Hambrey, M.J. (1982) Late Precambrian diamictites of northeastern Svalbard. *Geological Magazine*, **119,** 527-551.
Hambrey, M.J. (1983) Correlation of Late Proterozoic tillites in the North Atlantic region and Europe. *Geological Magazine*, **120,** 209-232.
Hambrey, M.J. (1994) *Glacial environments*. UCL Press, London, Glacial Environments pp.
Hambrey, M.J. and Glasser, N.F. (2012) Discriminating glacier thermal and dynamic regimes in the sedimentary record. *Sedimentary Geology*, **251–252,** 1-33.
Hambrey, M.J., Harland, W.B. and Waddams, P. (1981) Late Precambrian tillites in Svalbard. In: *Earth's pre-Pleistocene Glacial record* (Eds M.J. Hambrey and W.B. Harland). Cambridge University Press, Cambridge.

Hambrey, M.J. and McKelvey, B. (2000) Neogene fjordal sedimentation on the western margin of the Lambert Graben, East Antarctica. *Sedimentology*, **47,** 577-607.
Harland, W. (1971) Tectonic transpression in Caledonian Spitsbergen. *Geological Magazine*, **108,** 27-41.
Harland, W.B. (1964) Critical evidence for a great Infra-Cambrian glaciation. *Geologische Rundschau*, **54,** 45-61.
Harland, W.B., Hambrey, J.M. and Waddams, P. (1993) *Vendian geology of Svalbard*. Norsk polarinstitutt.
Harland, W.B. and Rudwick, M.J. (1964) The great infra-Cambrian ice age. *Scientific American*, **211,** 28-36.
Harland, W.B., Scott, R.A., Auckland, K.A. and Snape, I. (1992) The Ny Friesland Orogen, Spitsbergen. *Geological Magazine*, **129,** 679-707.
Hart, J.K. (1998) The deforming bed/debris-rich basal ice continuum and its implications for the formation of glacial landforms (flutes) and sediments (melt-out till). *Quaternary Science Reviews*, **17,** 737-754.
Hart, J.K. and Boulton, G.S. (1991) The interrelation of glaciotectonic and glaciodepositional processes within the glacial environment. *Quaternary Science Reviews*, **10,** 335-350.
Hart, J.K. and Roberts, D.H. (1994) Criteria to distinguish between subglacial glaciotectonic and glaciomarine sedimentation, I. Deformation styles and sedimentology. *Sedimentary Geology*, **91,** 191-213.
Herrington, P.M. and Fairchild, I.J. (Eds)(1989) *Carbonate shelf and slope facies evolution prior to Vendian glaciation, central East Greenland*. Graham Trotman, London, 285-297 pp.
Hoffman, P.F. (2009) Pan-glacial—a third state in the climate system. *Geology Today*, **25,** 100-107.
Hoffman, P.F., Halverson, G.P., Domack, E.W., Maloof, A.C., Swanson-Hysell, N.L. and Cox, G.M. (2012) Cryogenian glaciations on the southern tropical paleomargin of Laurentia (NE Svalbard and East Greenland), and a primary origin for the upper Russøya (Islay) carbon isotope excursion. *Precambrian Research*, **206–207,** 137-158.
Hoffman, P.F., Kaufman, A.J., Halverson, G.P. and Schrag, D.P. (1998) A Neoproterozoic snowball earth. *Science*, **281,** 1342.
Hoffmann, K. and Piotrowski, J.A. (2001) Till mélange at Amsdorf, central Germany: sediment erosion, transport and deposition in a complex, soft-bedded subglacial system. *Sedimentary Geology*, **140,** 215-234.
Hooyer, T.S., Iverson, N.R., Lagroix, F. and Thomason, J.F. (2008) Magnetic fabric of sheared till: A strain indicator for evaluating the bed deformation model of glacier flow. *Journal of Geophysical Research*, **113,** 1-15.
Iverson, N.R., Hooyer, T.S., Thomason, J.F., Graesch, M. and Shumway, J.R. (2008) The experimental basis for interpreting particle and magnetic fabrics of sheared till. *Earth Surface Processes and Landforms*, **33,** 627-645.
Jelínek, V. (1981) Characterization of the magnetic fabric of rocks. *Tectonophysics*, **79,** T63-T67.
Knoll, A., Hayes, J., Kaufman, A., Swett, K. and Lambert, I. (1986) Secular variation in carbon isotope ratios from Upper Proterozoic successions of Svalbard and East Greenland.
Kulling, O. (1934) Scientific results of the Swedish^ Norwegian arctic expedition in the summer of 1931. *Geografiska Annaler*, **16,** 161-253.
Laberg, J.S. and Vorren, T.O. (1995) Late Weichselian submarine debris flow deposits on the Bear Island Trough Mouth Fan. *Marine Geology*, **127,** 45-72.
Le Heron, D.P., Busfield, M.E. and Collins, A.S. (2013) Bolla Bollana boulder beds: A Neoproterozoic trough mouth fan in South Australia? *Sedimentology*.
Le Heron, D.P., Sutcliffe, O.E., Whittington, R.J. and Craig, J. (2005) The origins of glacially related soft-sediment deformation structures in Upper Ordovician glaciogenic rocks: implication for ice-sheet dynamics. *Palaeogeography, Palaeoclimatology, Palaeoecology*, **218,** 75-103.

Lukas, S., Benn, D.I., Boston, C.M., Brook, M., Coray, S., Evans, D.J.A., Graf, A., Kellerer-Pirklbauer, A., Kirkbride, M.P., Krabbendam, M., Lovell, H., Machiedo, M., Mills, S.C., Nye, K., Reinardy, B.T.I., Ross, F.H. and Signer, M. (2013) Clast shape analysis and clast transport paths in glacial environments: A critical review of methods and the role of lithology. *Earth-Science Reviews*, **121,** 96-116.
Lyberis, N. and Manby, G. (1993) The origin of the West Spitsbergen Fold Belt from geological constraints and plate kinematics: implications for the Arctic. *Tectonophysics*, **224,** 371-391.
Mark, D.M. (1973) Analysis of Axial Orientation Data, Including Till Fabrics. *Geological Society of America Bulletin*, **84,** 1369-1374.
Menzies, J. (2000) Micromorphological analyses of microfabrics and microstructures indicative of deformation processes in glacial sediments. *Geological Society London Special Publications*, **176,** 245.
Miall, A.D. (1977) A review of the braided-river depositional environment. *Earth-Science Reviews*, **13,** 1-62.
Moncrieff, A.C.M. (1989) Classification of poorly-sorted sedimentary rocks. *Sedimentary Geology*, **65,** 191-194.
Moncrieff, A.C.M. and Hambrey, M.J. (1988) Late precambrian glacially-related grooved and striated surfaces in the Tillite Group of Central East Greenland. *Palaeogeography, Palaeoclimatology, Palaeoecology*, **65,** 183-200.
Phillips, E., Everest, J. and Reeves, H. (2013) Micromorphological evidence for subglacial multiphase sedimentation and deformation during overpressurized fluid flow associated with hydrofracturing. *Boreas*, **42,** 395-427.
Phillips, E.R., Evans, D.J.A. and Auton, C.A. (2002) Polyphase deformation at an oscillating ice margin following the Loch Lomond Readvance, central Scotland, UK. *Sedimentary Geology*, **149,** 157-182.
Powell, R.D. (1984) Glacimarine processes and inductive lithofacies modelling of ice shelf and tidewater glacier sediments based on Quaternary examples. *Marine Geology*, **57,** 1-52.
Powell, R.D. (1990) Glacimarine processes at grounding-line fans and their growth to ice-contact deltas. *Geological Society, London, Special Publications*, **53,** 53-73.
Riedel, W. (1929) Zur Mechanik geologischer Brucherscheinungen. *Zentralblatt für Geologie und Paleontologie***,** 354-368.
Shumway, J.R. and Iverson, N.R. (2009) Magnetic fabrics of the Douglas Till of the Superior lobe: exploring bed-deformation kinematics. *Quaternary Science Reviews*, **28,** 107-119.
Sneed, E.D. and Folk, R.L. (1958) Pebbles in the lower Colorado River, Texas a study in particle morphogenesis. *The Journal of Geology***,** 114-150.
Stupavsky, M. and Gravenor, C.P. (1975) Magnetic fabric around boulders in till. *Bulletin of the Geological Society of America*, **86,** 1534-1536.
Syvitski, J.P.M., Andrews, J.T. and Dowdeswell, J.A. (1996) Sediment deposition in an iceberg-dominated glacimarine environment, East Greenland: basin fill implications. *Global and Planetary Change*, **12,** 251-270.
Thomason, J.F. and Iverson, N.R. (2009) Deformation of the Batestown till of the Lake Michigan lobe, Laurentide ice sheet. *Journal of Glaciology*, **55,** 131-146.
van der Meer, J.M. (1993) Microscopic evidence of subglacial deformation. *Quaternary Science Reviews*, **12,** 553-587.
van der Wateren, F.M. (2002) Processes of glaciotectonism. In: *Modern and Past Glacial Environments* (Ed J. Menzies), pp. 417-443. Butterworth-Heinemann, Oxford.
Waller, R.I., Phillips, E.R., Murton, J., Lee, J.R. and Whiteman, C. (2011) Sand intraclasts as evidence of subglacial deformation of Middle Pleistocene permafrost, North Norfolk, UK. *Quaternary Science Reviews*, **30,** 3481-3500.
Wilson, C.B. and Harland, W.B. (1964) The Polarisbreen Series and other evidences of late Pre-Cambrian ice ages in Spitsbergen. *Geological Magazine*, **101,** 198-219.

Facies association	Description	Lithofacies codes	Interpretation
Diamictite and conglomerates (A-1)	Massive and stratified diamictites, consisting of poorly-sorted, subangular to subrounded, intrabasinal and extrabasinal clasts in a fine-grained sandy matrix, sometimes with a well-pronounced haematite staining. Intercalated with lenses of conglomerate, sometimes displaying channel geometries	**Dm** **Ds** **Gm** **Gs** *Sm* *Ss*	Subaqueous deposition from either: (i) rainout from a high concentration of debris-rich icebergs; or (ii) from sediment-laiden efflux jets at close to the grounding line of a glacier or ice-sheet. Conglomerate facies represent erosional lags or mass flow deposits. In places (for example, at Dracoisen), the sediment architecture suggests deposition as a grounding-line fan
Lenticular and tabular sandstones (A-2)	Pale yellow to greenish-grey, moderate to well-sorted sandstones, consisting of quartz with minor feldspar and lithic fragments. Bed thickness is normally 0.1 to 4.0 m thick and can display either channel-like and lenticular or tabular geometries. Rare cross-bedding and ripple lamination	**Sm** **Ss** *Dm* *Ds* *Gm* *Gs*	Proximal subaqueous deposition through the release of debris from subglacial conduits at the grounding-line fan, which can progress into subaqueous channels in a more distal location. Tabular sandstones are interpreted as deposition as a subaqueous outwash fan

Facies association	Description	Lithofacies codes	Interpretation
Deformed rhythmites (B-1)	Intercalated silt–sand–carbonate rhythmites exhibiting both ductile (recumbent folds) and brittle (normal and reverse offset faulting and brecciation) deformation. Exhibits an increase in intensity of deformation towards the top. Often overlain by massive diamictite with intraclasts and lenses of the underlying rhythmite	**Fl(d)** *Dm* *Dm(d)* *Fl*	Quiescent subaqueous sedimentation during an ice retreat phase. Overridden by grounded ice during an ice advance phase and glaciotectonised by an ice advance to the north. The increase in apparent deformation reflects strain profile through the sediment. Rhythmite lenses are interpreted as rafts, dislocated from underlying sediments and emplaced within a subglacial till
Diamictites (B-2)	Massive diamictite, occasionally exhibiting deformed stratification (Fig. 8B) showing strong, consistent clast fabric and AMS fabrics. Predominantly sub-rounded to subangular clasts (low Ra-RWR; Fig. 11). Often associated with lenticular sandstone and conglomerate (below)	**Dm** **Dm(d)** *Sm(d)* *Ss(d)* *Fl(d)* *Fm(d)*	Subglacial debris originating through subglacial erosion and transportation. When associated with other subglacial facies, massive diamictites are interpreted as subglacial tills deposited by grounded ice. If associated with glacio-aqueous facies it may also form in subaqueous environment
Lenticular sandstones and conglomerates (B-3)	Lens shaped sandstone and conglomerate bodies (<1 to 5 m thick) occurring with massive diamictite. Sometimes show internal stratification with cross-stratification and rare climbing ripples. Commonly show visible disruption around margins such as folding and faulting. Surrounding diamictite often envelops the lens	**Gm(d), Gs(d)** **Sm(d), Ss(d)** *Fl(d)* *Fm(d)* *Dm* *Dm(d)*	Subglacial channel deposits during ice-grounding. Deposits may have initially eroded into underlying sediments. Subsequently deformed and sheared during as part of the subglacial till mosaic
Boulder pavements (B-4)	Prominent surfaces within otherwise massive diamictites containing a high proportion of large (>10 cm diameter) clasts with consistent striations (north-west/south-east). Clasts commonly display stoss-and-lee forms, often with a faceted upper surface. Strong, consistent AMS and	**Gm** *Dm* *Dm(d)*	Formed through subglacial deposition and erosion by either: (i) a period of erosion at the ice-bed interface and faceting and realignment of clasts because of the overriding ice; or (ii) decoupling within the bed at a décollement surface, within sediment

	clast fabrics		

										Eignevectors						Eigenvalues					
Fabric	**Latitude/longitude**		**Lithology**	**No**	**Location**	**Unit**	**FA**	**Bedding**		**S_1**		**S_2**		**S_3**		**S_1**	**S_2**	**S_3**	**I**	**E**	
F9	79.20549	18.4023	Diamictite	50	Dracoisen	W1	**A-1**	343	51	184	4	86	61	276	29	0.527	0.4161	0.0582	0.11044	0.21044	
F10	79.2055	18.4025	Diamictite	50	Dracoisen	W1	U	343	51	168	22	60	38	281	44	0.6537	0.2849	0.0614	0.09393	0.56417	
F13	79.21481	18.3997	Diamictite	50	Dracoisen	W2	**A-1**	342	50	343	1	75	55	363	46	0.4676	0.3144	0.218	0.46621	0.32763	
F14	79.20561	18.4047	Diamictite	50	Dracoisen	W2	**A-1**	326	40	174	16	82	8	328	72	0.5393	0.3656	0.095	0.17615	0.32208	
F15	79.20479	18.4111	Diamictite	50	Dracoisen	W1	**A-1**	338	40	151	19	37	48	155	35	0.5885	0.3496	0.0619	0.10518	0.40595	
F17	79.20561	18.4047	Diamictite	50	Dracoisen	W2	**A-1**	320	65	144	40	17	35	264	30	0.4956	0.3337	0.1707	0.34443	0.32667	
F1	79.083677	18.41481	Diamictite	50	Ditlovtoppen	W3	**A-1**	003	30	320	0	230	13	51	77	0.5221	0.3589	0.1189	0.22773	0.31258	
F4	79.0794574	18.39083	Diamictite	50	Ditlovtoppen	W1	A-1	26	32	44	10	139	26	296	62	0.4684	0.4188	0.1128	0.24082	0.10589	
F5	79.08309	18.4135	Diamictite	50	Ditlovtoppen	W3	B-2	003	30	162	23	65	17	302	61	0.6081	0.2988	0.0931	0.1531	0.50863	
F6	79.08236	18.4111	Diamictite	50	Ditlovtoppen	W3	B-2	003	30	184	14	81	42	289	45	0.6053	0.3256	0.0691	0.11416	0.46208	
F7	79.08019	18.403	Diamictite	50	Ditlovtoppen	W3	B-2	004	42	136	30	39	13	289	57	0.6976	0.2658	0.0366	0.05247	0.61898	
F3	79.0832	18.4129	Diamictite	50	Ditlovtoppen	W3	B-2	020	32	200	6	292	10	81	79	0.6584	0.252	0.0897	0.13624	0.61725	
F2	79.0832	18.4129	Diamictite	50	Ditlovtoppen	W3	B-2	003	30	178	5	84	32	276	57	0.7026	0.2179	0.0795	0.11315	0.68987	
F22	78.9386	18.440	Diamictite	50	Andromedafjellet	W1	A-1	247	48	150	17	258	46	45	39	0.5717	0.2388	0.1895	0.33147	0.5823	
F21	78.9383	18.433	Diamictite	50	Andromedafjellet	W3	**B-2**	253	40	192	10	285	13	67	74	0.4809	0.3801	0.139	0.28904	0.20961	

Site	**.atitude/longitude**		**Lithology**	**FA**	**Location**	**Unit**	**Bedding**	**Dip**	**No**	**Km (SI)**	**K_1**		***K_1 95% Error***		**K_2**		***K_2 95% Error***		**K_3**		***K_3 95% Error***		**L**	**F**	**P_j**	**T**
DC2	79.2055	18.4020	**Diamictite**	A	Dracoisen	**W1**	343	51	18	336	**350**	**31**	*32*	*11*	**122**	**48**	*32*	*20*	**243**	**25**	*21*	*12*	1.003	1.005	1.008	0.273
DC5	79.2057	18.4056	**Carbonate**	A	Dracoisen	**W2**	341	51	6	123	**194**	**6**	*51*	*9*	**106**	**16**	*51*	*17*	**308**	**73**	*21*	*13*	1.001	1.002	1.003	0.090
DC57	79.2153	18.3980	**Diamictite**	A	Dracoisen	**W3**	334	43	10	272	**132**	**28**	*27*	*7*	**27**	**26**	*27*	*15*	**261**	**50**	*16*	*7*	1.004	1.006	1.010	0.251
DC6	79.2056	18.4073	**Rhythmites**	A	Dracoisen	**W2**	341	51	11	188	**131**	**38**	*62*	*17*	**20**	**25**	*62*	*23*	**266**	**43**	*27*	*15*	1.002	1.024	1.026	-0.844
DC61	79.2153	18.3979	**Diamictite**	A	Dracoisen	**W2**	341	51	17	198	**151**	**22**	*16*	*7*	**50**	**25**	*22*	*16*	**277**	**55**	*23*	*5*	1.004	1.008	1.013	0.299
DC62	79.2153	18.3979	**Diamictite**	A	Dracoisen	**W3**	341	51	10	216	**355**	**4**	*24*	*13*	**86**	**17**	*26*	*15*	**254**	**73**	*22*	*9*	1.004	1.009	1.014	0.448
DC63	79.2153	18.3982	**Diamictite**	A	Dracoisen	**W3**	341	51	18	260	**9**	**25**	*25*	*6*	**133**	**40**	*24*	*7*	**254**	**32**	*7*	*6*	1.002	1.011	1.015	0.657
DC65	79.2151	18.4003	**Diamictite**	A	Dracoisen	**W3**	330	46	18	50	**23**	**47**	*41*	*15*	**114**	**2**	*45*	*35*	**206**	**43**	*40*	*17*	1.003	1.002	1.005	-0.096
DC7	79.2058	18.4082	**Carbonate**	A	Dracoisen	**W3**	341	51	11	239	**123**	**2**	*64*	*9*	**33**	**3**	*64*	*14*	**239**	**87**	*20*	*8*	1.002	1.009	1.012	0.663
DF25	79.0816	18.4104	**Diamictite**	A	Ditlovtoppen	**W3**	004	42	15	357	**133**	**50**	*62*	*10*	**3**	**29**	*62*	*15*	**258**	**26**	*17*	*11*	1.001	1.021	1.025	0.900
DF26	79.0815	18.4103	**Diamictite**	A	Ditlovtoppen	**W3**	001	30	9	368	**176**	**17**	*30*	*9*	**75**	**34**	*30*	*10*	**288**	**51**	*10*	*9*	1.004	1.015	1.021	0.557
DF29	79.0809	18.4079	**Rhythmites**	B1	Ditlovtoppen	**W2**	003	30	15	197	**146**	**20**	*39*	*3*	**46**	**26**	*39*	*5*	**269**	**56**	*11*	*3*	1.002	1.029	1.035	0.881
DF30	79.0809	18.4079	**Rhythmites**	B1	Ditlovtoppen	**W2**	003	30	13	147	**174**	**10**	*8*	*2*	**78**	**28**	*9*	*3*	**282**	**60**	*5*	*2*	1.004	1.036	1.045	0.799
DF31	79.0807	18.4077	**Diamictite**	B	Ditlovtoppen	**W3**	002	39	16	395	**139**	**38**	*37*	*8*	**31**	**21**	*38*	*15*	**279**	**45**	*17*	*7*	1.004	1.012	1.016	0.536
DF32	79.0807	18.4077	**Diamictite**	B	Ditlovtoppen	**W3**	002	39	11	446	**98**	**44**	*57*	*16*	**189**	**1**	*57*	*16*	**280**	**46**	*17*	*16*	1.003	1.009	1.013	0.477
DFB2A	79.0819	18.4093	**Diamictite**	B	Ditlovtoppen	**W1**	004	42	7	186	**159**	**34**	*15*	*2*	**29**	**43**	*15*	*12*	**269**	**28**	*12*	*2*	1.004	1.008	1.012	0.396
DFB4D	79.0833	18.4129	**Rhythmites**	B1	Ditlovtoppen	**W3**	004	42	12	435	**351**	**14**	*16*	*7*	**92**	**40**	*25*	*7*	**256**	**47**	*25*	*10*	1.007	1.005	1.011	-0.152
DFB4F	79.0833	18.4129	**Rhythmites**	B	Ditlovtoppen	**W3**	004	42	8	579	**186**	**11**	*44*	*7*	**86**	**39**	*44*	*9*	**289**	**49**	*12*	*7*	1.004	1.023	1.029	0.676
EFA121	78.9528	18.4257	**Sandstone**	B1	Andromedafjel	**W2**	253	40	12	171	**263**	**42**	*16*	*4*	**160**	**14**	*16*	*7*	**55**	**45**	*7*	*5*	1.005	1.003	1.008	-0.273
EFA128	78.9528	18.4257	**Diamictite**	B	Andromedafjel	**W3**	251	40	7	409	**154**	**24**	*16*	*3*	**259**	**30**	*15*	*2*	**32**	**50**	*4*	*2*	1.005	1.020	1.027	0.578
EFA146	78.9528	18.4257	**Diamictite**	B	Andromedafjel	**W3**	251	40	11	561	**190**	**22**	*12*	*6*	**296**	**34**	*13*	*6*	**74**	**48**	*9*	*5*	1.008	1.010	1.018	0.108
EFA10	78.9383	18.4281	**Sandstone**	A	Reinsryggen	**W3**	256	40	9	496	**322**	**18**	*14*	*4*	**222**	**27**	*16*	*6*	**82**	**57**	*10*	*5*	1.006	1.011	1.018	0.261
EFA103	78.9383	18.4325	**Diamictite**	A	Reinsryggen	**W3**	256	40	12	533	**298**	**12**	*12*	*5*	**31**	**13**	*16*	*12*	**165**	**74**	*16*	*4*	1.013	1.017	1.031	0.116
EFA92	78.9383	18.4325	**Diamictite**	B	Reinsryggen	**W3**	253	40	11	227	**190**	**17**	*7*	*5*	**287**	**20**	*7*	*5*	**64**	**63**	*6*	*4*	1.007	1.008	1.015	0.087

Site	No	Location	FA	S_1	S_2	S_3	I	E
DC2	18	Dracoisen	A	0.7722	0.1725	0.0553	0.071614	0.776612
DC5	6	Dracoisen	A	0.7069	0.2647	0.0284	0.040175	0.625548
DC57	10	Dracoisen	A	0.8899	0.095	0.0151	0.016968	0.893246
DC6	11	Dracoisen	A	0.761	0.219	0.0201	0.026413	0.712221
DC61	17	Dracoisen	A	0.8574	0.1084	0.0343	0.040005	0.873571
DC62	10	Dracoisen	A	0.8176	0.1325	0.0499	0.061032	0.83794
DC63	18	Dracoisen	A	0.8137	0.1754	0.0109	0.013396	0.784441
DC65	18	Dracoisen	A	0.7226	0.2155	0.0619	0.085663	0.701771
DC7	11	Dracoisen	A	0.523	0.4114	0.0656	0.12543	0.213384
DF25	15	Ditlovtoppen	A	0.6198	0.3147	0.0655	0.105679	0.492256
DF26	9	Ditlovtoppen	A	0.7047	0.2764	0.0188	0.026678	0.607776
DF29	15	Ditlovtoppen	B1	0.6218	0.3702	0.008	0.012866	0.404632
DF30	13	Ditlovtoppen	B1	0.9705	0.0284	0.0011	0.001133	0.970737
DF31	16	Ditlovtoppen	B	0.5898	0.3232	0.087	0.147508	0.452018
DF32	11	Ditlovtoppen	B	0.6054	0.3706	0.024	0.039643	0.387843
DFB2A	7	Ditlovtoppen	B	0.9422	0.0562	0.0015	0.001592	0.940352
DFB4D	12	Ditlovtoppen	B1	0.9226	0.0686	0.0089	0.009647	0.925645
DFB4F	8	Ditlovtoppen	B	0.6529	0.3289	0.0181	0.027722	0.496248
EFA121	12	Andromedafjellet East	B1	0.9548	0.04	0.0052	0.005446	0.958106
EFA128	7	Andromedafjellet East	B	0.9101	0.0877	0.0022	0.002417	0.903637
EFA146	11	Andromedafjellet East	B	0.9522	0.0379	0.0099	0.010397	0.960197
EFA10	9	Reinsryggen	A	0.9407	0.0533	0.006	0.006378	0.94334
EFA103	12	Reinsryggen	A	0.8997	0.0943	0.0059	0.006558	0.895187
EFA92	11	Reinsryggen	B	0.9802	0.0145	0.0053	0.005407	0.985207

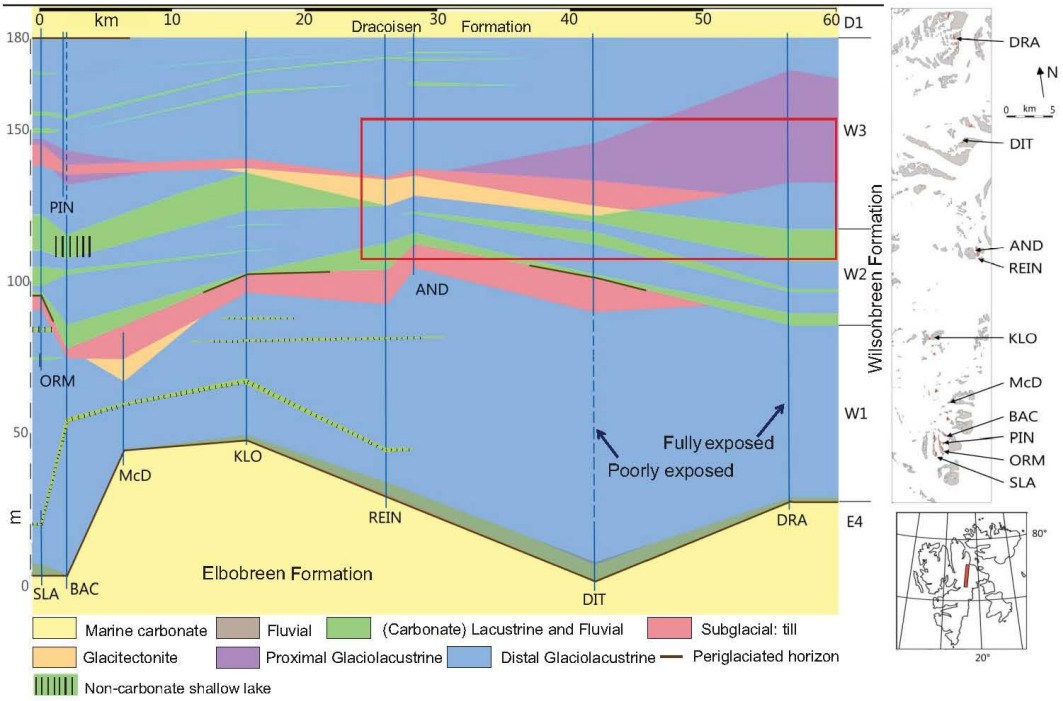

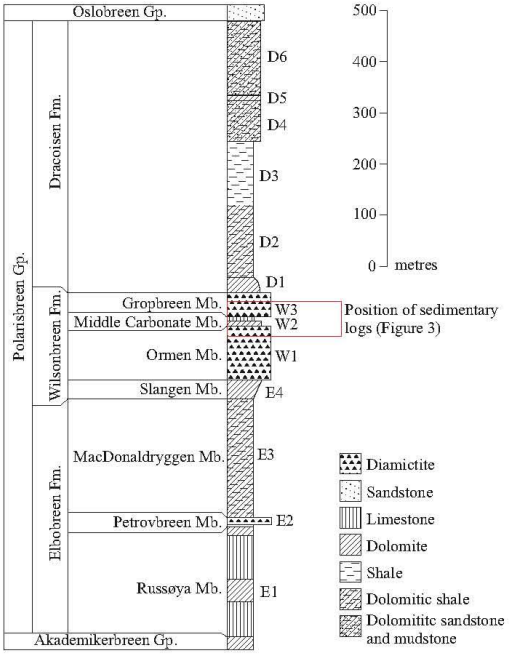

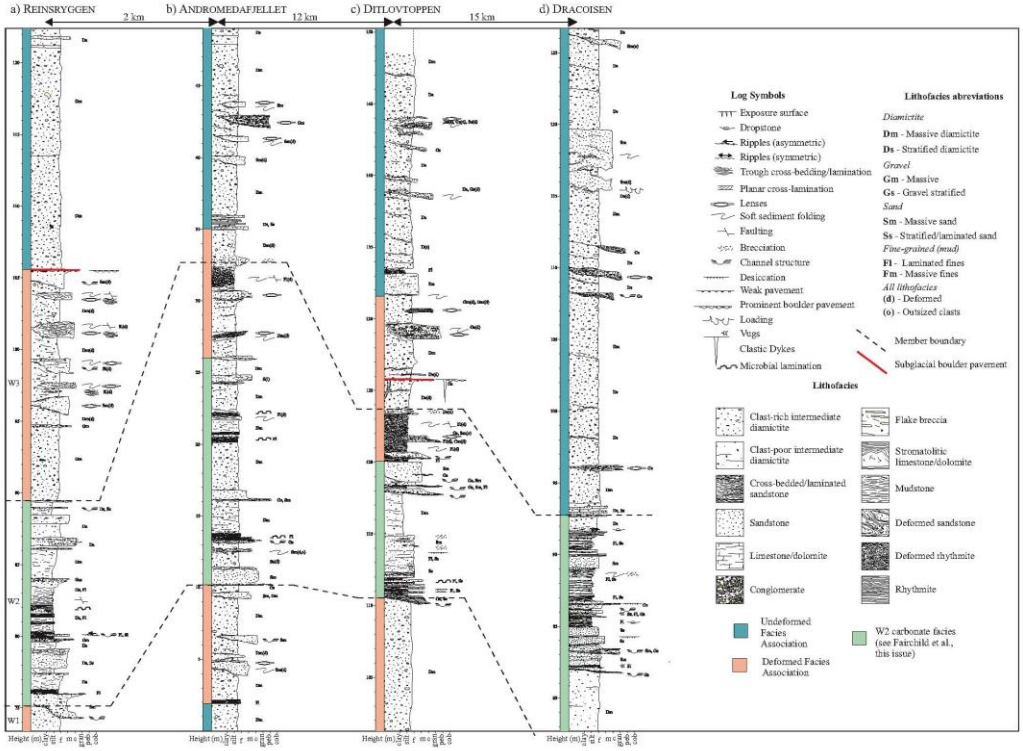

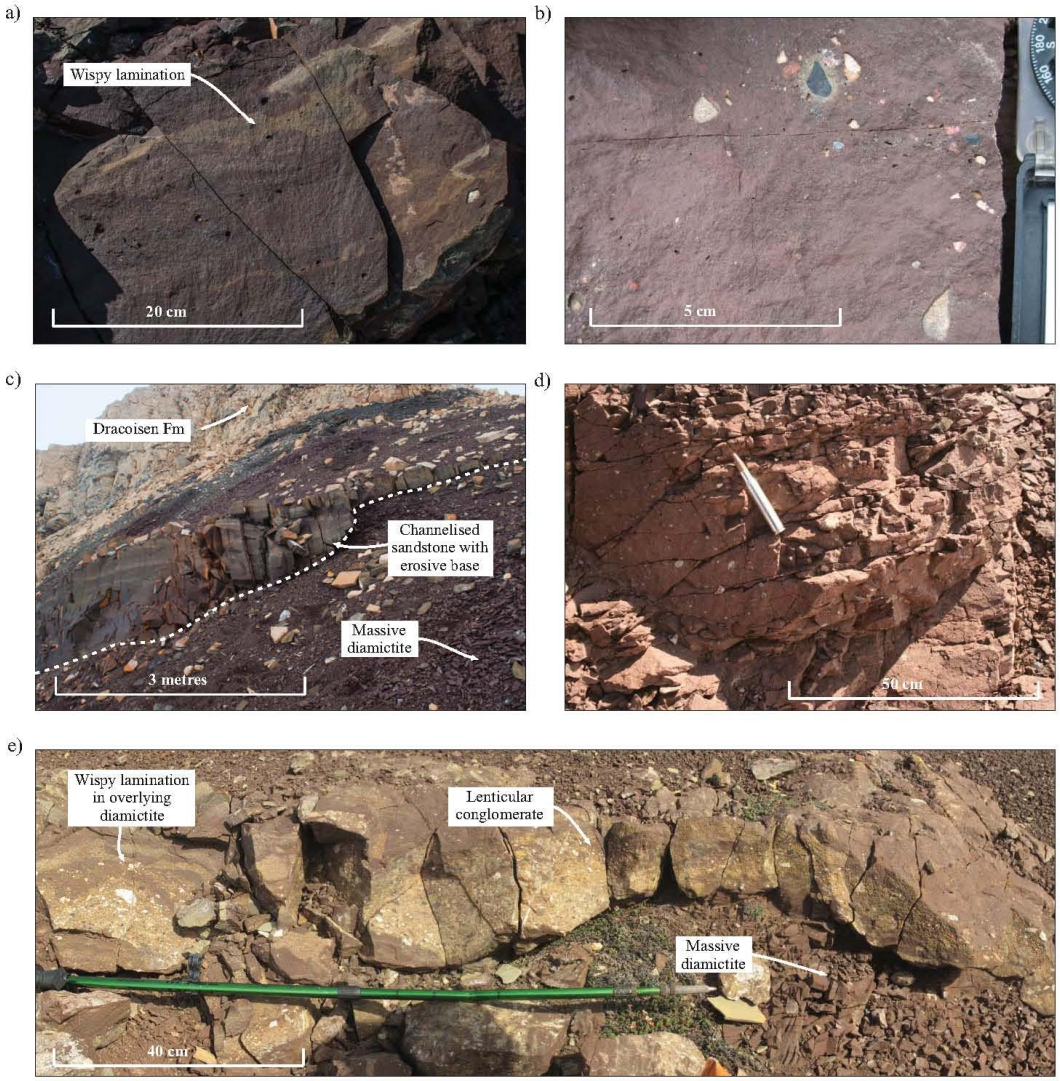

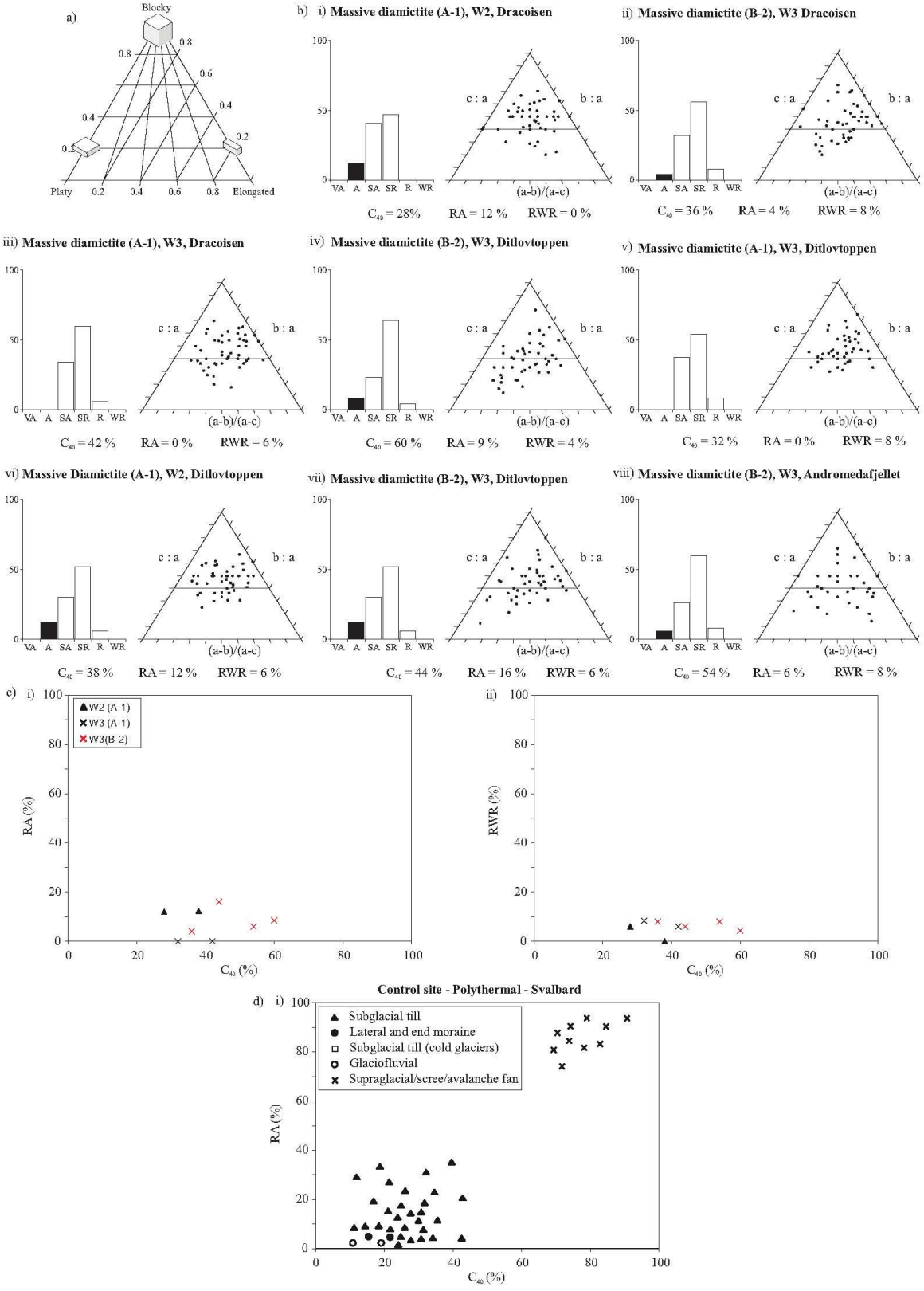

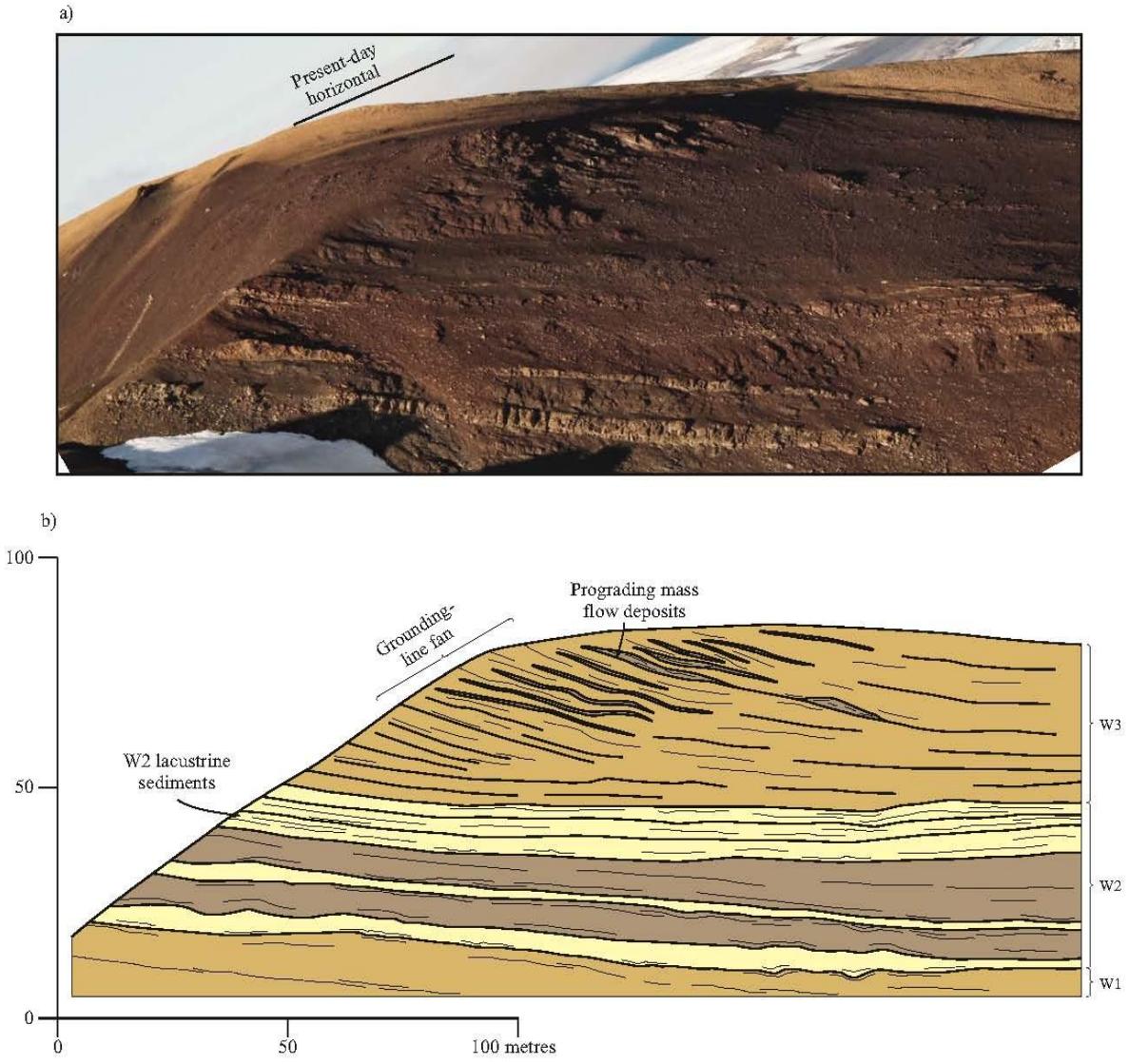

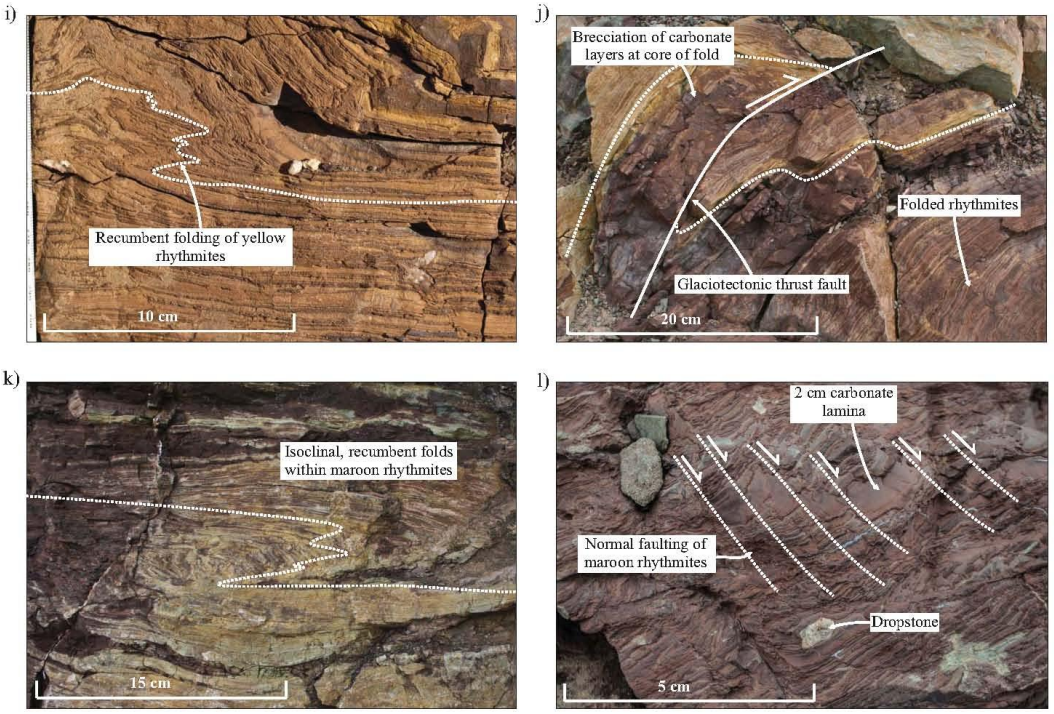

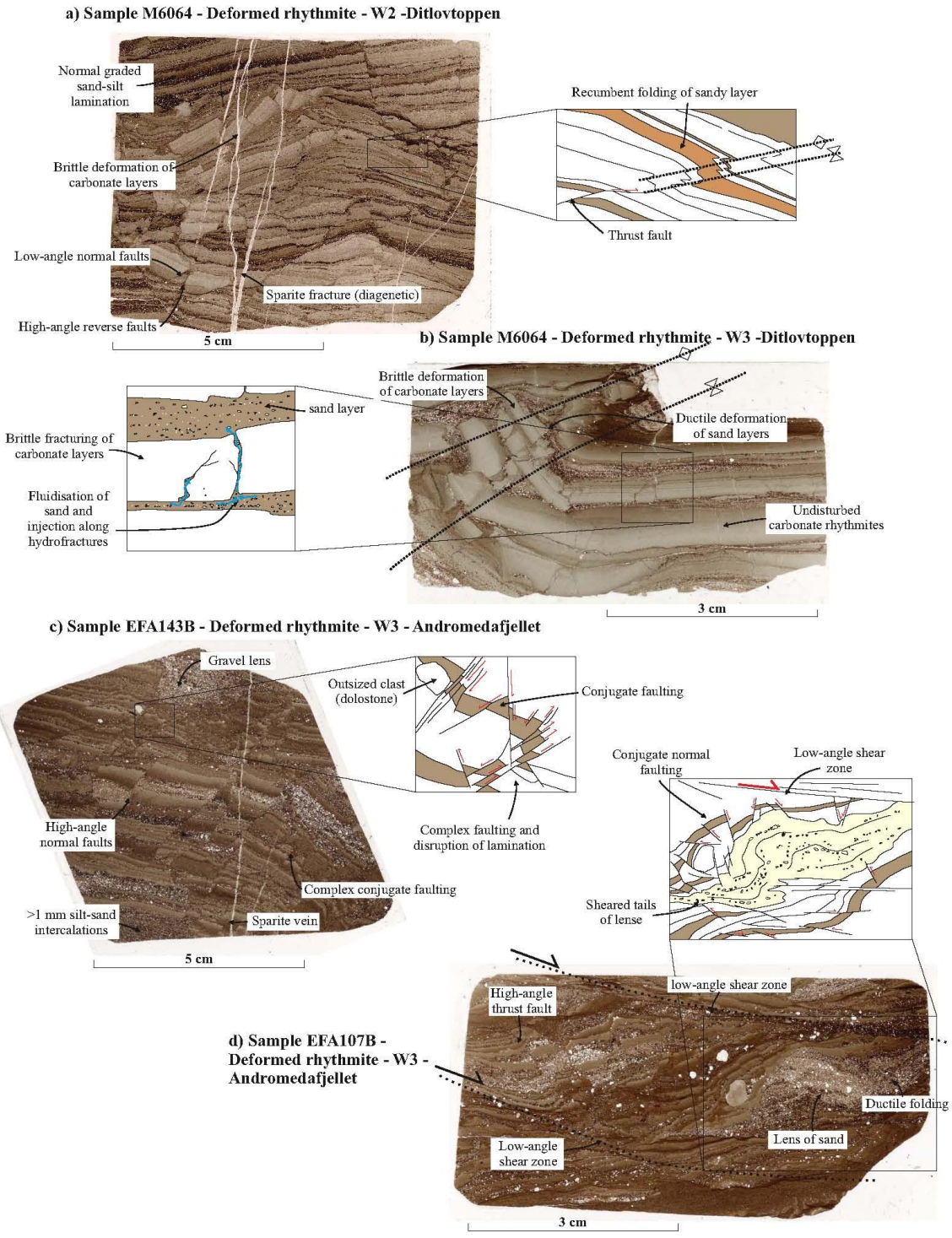

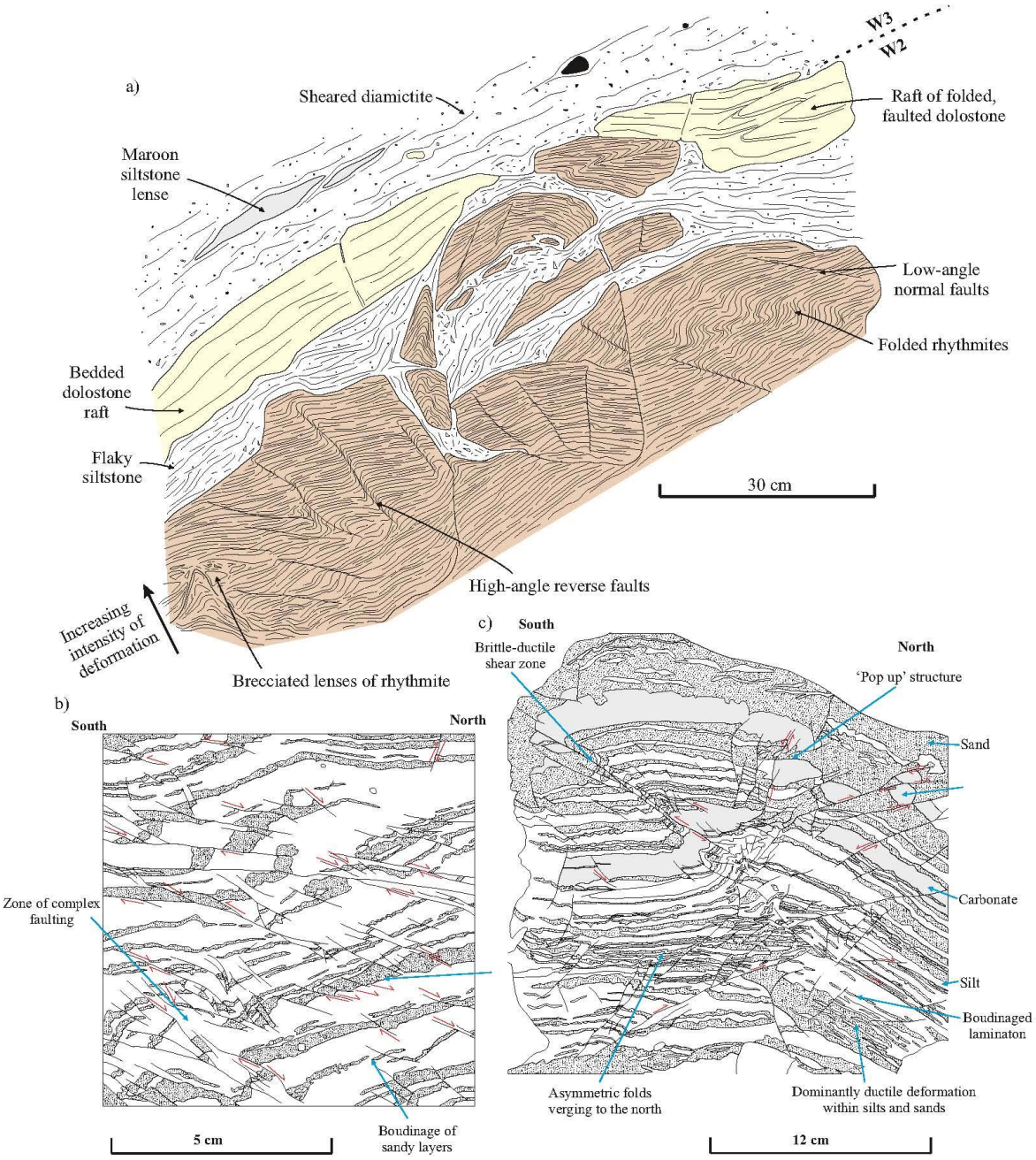

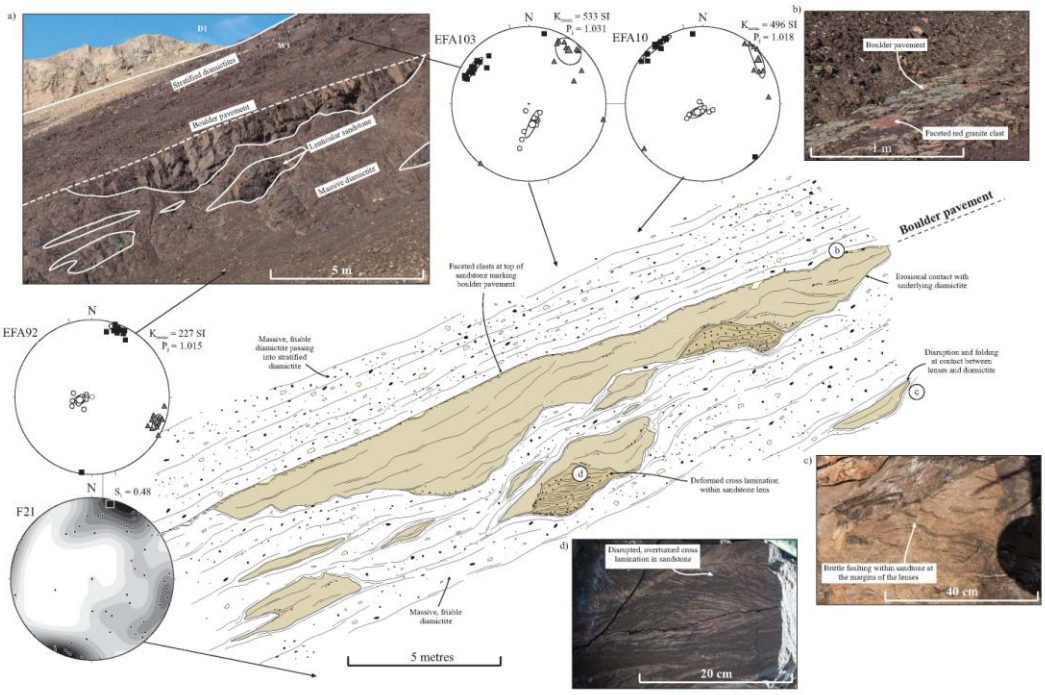

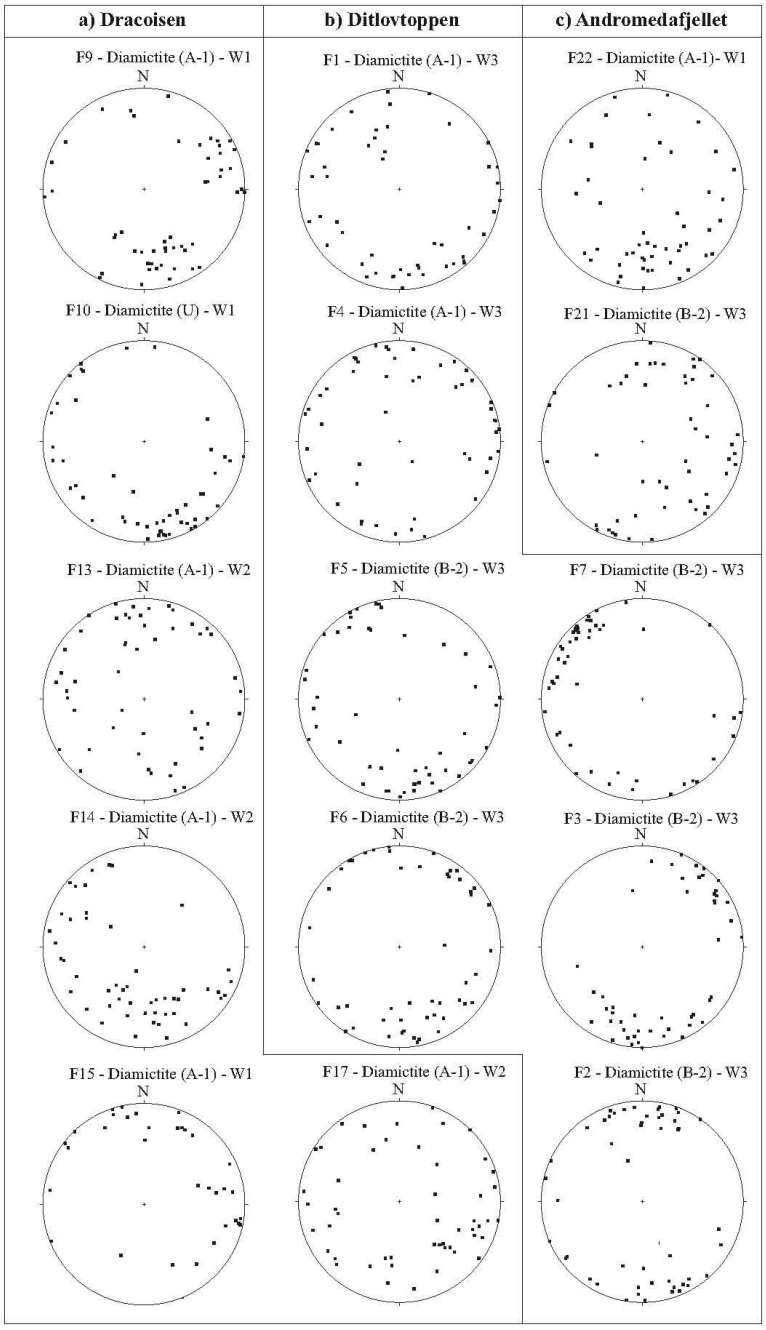

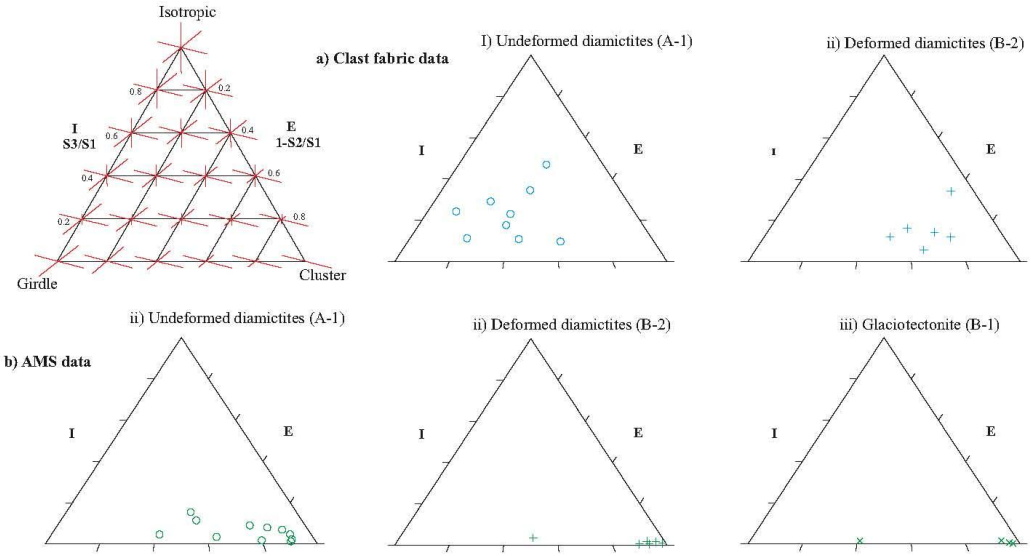

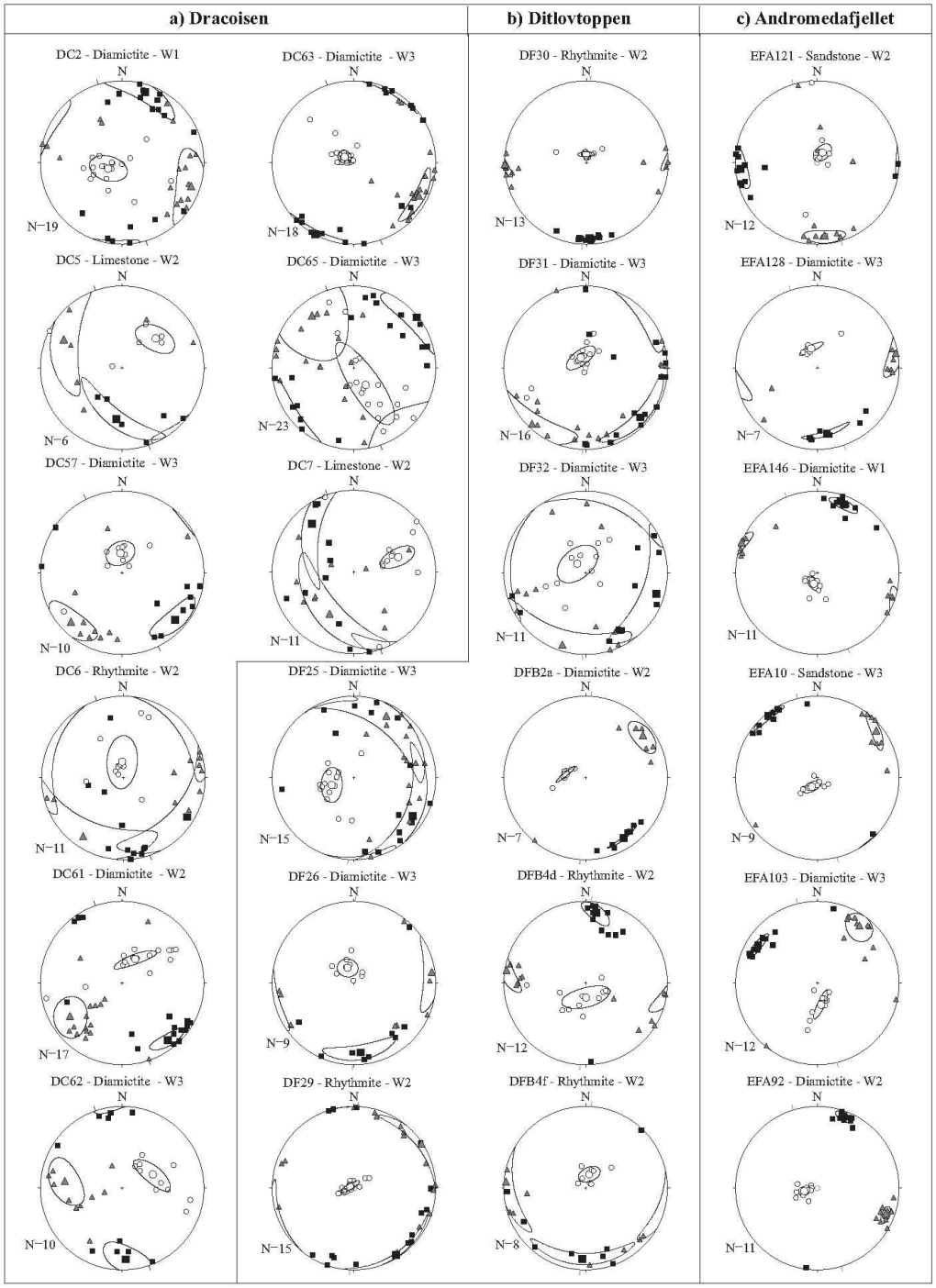

SUMMARY OF THE DEFORMATIONAL FACIES ASSOCIATIONS